

Prediction of triaxial behavior of recycled aggregate concrete using multivariable regression and artificial neural network techniques



Jinjun Xu^a, Yuliang Chen^b, Tianyu Xie^{c,*}, Xinyu Zhao^{d,*}, Beibei Xiong^a, Zongping Chen^e

^aCollege of Civil Engineering, Nanjing Tech University, Nanjing 211816, China

^bCollege of Civil Engineering, Guangxi University of Science and Technology, Liuzhou 545006, China

^cSchool of Civil, Environmental and Mining Engineering, University of Adelaide, Adelaide, SA 5005, Australia

^dState Key Laboratory of Subtropical Building Science, South China University of Technology, Guangzhou 510640, China

^eKey Laboratory of Disaster Prevention and Structural Safety of China Ministry of Education, Guangxi University, Nanning 530004, China

HIGHLIGHTS

- Design-oriented models are developed to predict the RAC's triaxial behavior.
- Parametric sensitivity analysis is conducted using grey theory.
- The failure mechanism of RAC under triaxial load are evaluated.
- MNR and two ANN models are developed using the selected inputs and databases.
- The newly developed models show significantly improved accuracies.

ARTICLE INFO

Article history:

Received 26 November 2018

Received in revised form 20 June 2019

Accepted 17 July 2019

Available online 1 August 2019

Keywords:

Recycled aggregate concrete (RAC)

Triaxial behavior

Grey correlation analysis

Multiple nonlinear regression

Artificial neural networks

BP algorithm

Genetic algorithm

ABSTRACT

A cost-effective design of concrete elements in compliance with sustainability principles requires to accurately predict the behavior of concrete under various loading conditions. Yet to date available approaches for the prediction and evaluation of recycled aggregate concretes (RAC) under triaxial load are very scarce, which may hinder the transition of such an eco-friendly concrete from lab-based technique to widespread applications. As a first attempt to iron out this issue, this study develops some reliable and accurate analytical tools on the basis of an experimental database containing the results of 193 cylindrical peak stress under axisymmetric triaxial load, 55 cubic peak stress under true triaxial load, 76 peak strains and 61 elastic moduli of RAC retrieved from an extensive review of the literature. First, a new empirical design-oriented model is presented refining the generic form of conventional confinement models for natural aggregate concrete while considering the impacts of RCAs. Then Grey Correlation Analysis (GCA) is conducted to look into the sensitivity of the key parameters that affect the triaxial behavior of RAC. The results of the GCA indicate that the triaxial behavior of RAC mainly depends on the effective water-to-cement binder ratio, aggregate-to-cement ratio, lateral stress conditions, exposure temperature, as well as the RCA replacement ratio. Having the input parameters identified by the GCA, three robust data-mining mathematic tools, namely Multiple Nonlinear Regression (MNR), Artificial Neural Network (ANN), and hybrid Genetic Algorithm Artificial Neural Network (GA-ANN) are employed to simulate the mechanical performances of RAC under triaxial load. The results demonstrate that the developed MNR equations and the neural network models satisfactorily predict the behavior of RAC under triaxial load; among those models (including the developed design-oriented one), the ANN optimized with GA performs the best. These arguably point to the possibility of the application of those models in the design and evaluation of structural members manufactured using RAC, especially for them under complex loading scenarios.

© 2019 Elsevier Ltd. All rights reserved.

1. Introduction

Recycled concrete aggregates (RCAs) produced by crushing old concrete from construction and demolition (C&D) wastes can be

* Corresponding authors.

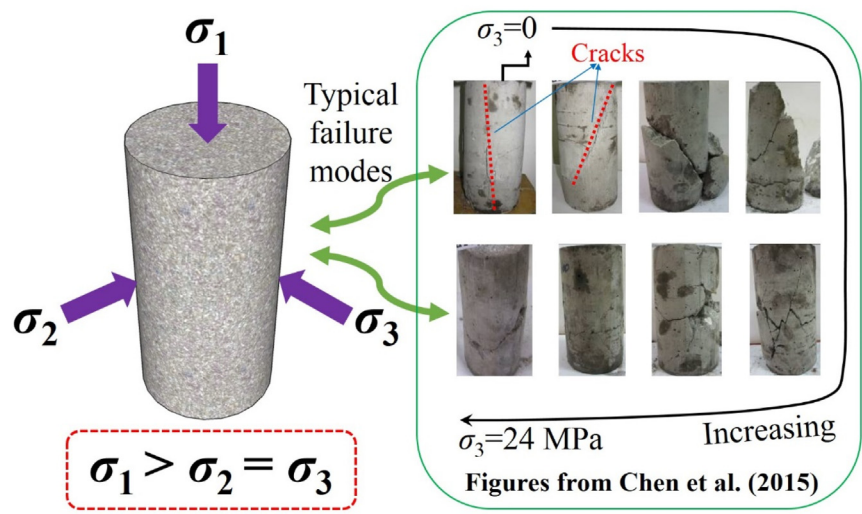
E-mail addresses: jixu_concrete@163.com (J. Xu), yichen616@163.com (Y. Chen), tianyu.xie@adelaide.edu.au (T. Xie), ctzhaoxy@scut.edu.cn (X. Zhao), zpchen@gxu.edu.cn (Z. Chen).

reused to replace natural aggregates (NAs) in new concrete to eliminate the environmental impacts of these C&D wastes [1–4]. The resulting engineered recycled aggregate concrete (RAC) is now widely recognized as a type of “Eco-friendly Concrete” [5–8], which can be a promising alternative to conventional NA-based concrete and has drawn increasing research attention in recent years.

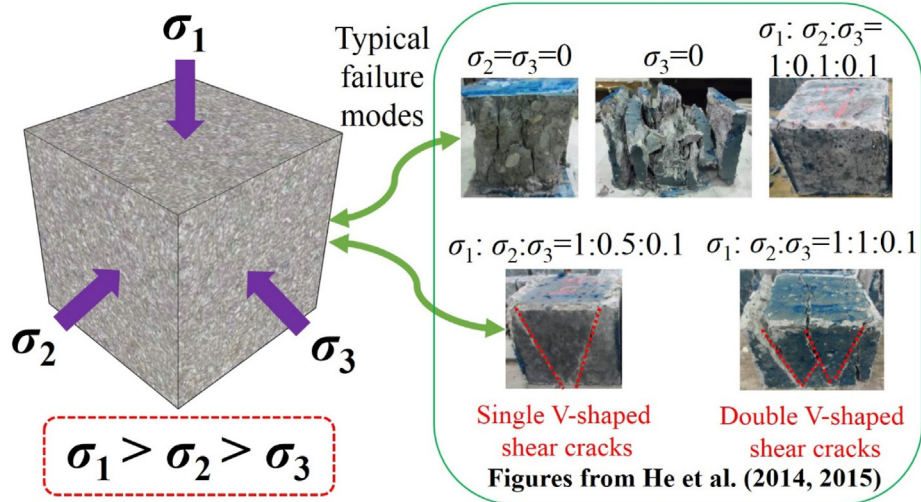
The research outcomes from a large volume of studies published in the past three decades have demonstrated the inferior properties of RCA compared to NA, such as high water absorption capacity, brittleness of the adhesive old mortar, weak bonding between old mortar and new mortar, cracks generated during crushing process (e.g., [9–17]). These deleterious aspects lead to a degree of reduction in the mechanical properties of RAC. Confining RAC with external steel tubes [17–19] or FRP laminates [20–22] is believed to enhance the mechanical properties of RAC; however, a great uncertainty arising from the use of RAC still exists, which at least means that the existing predictive equations or models developed specifically for natural aggregate concrete (NAC) could not be directly transferable to RAC.

The real mechanical state of concrete complicates the above-mentioned issues, where concrete is often subjected to multi-axial loadings when it has been structurally used. For instance, a spandrel concrete beam is expected to resist flexure and torsion simultaneously; similar examples are numerous. Undoubtedly, the combined action of forces greatly affects the structural behavior of concrete members. Hence, in order to achieve more reliable and cost-effective designs, it requires to accurately predict the mechanical performances of concrete under complex loading conditions.

A few studies hitherto [23–29] have been conducted to investigate the triaxial behavior of RAC, where two types of testing methods are commonly adopted, namely axisymmetric triaxial compressive tests and true triaxial compressive tests. The loading conditions of the two types are graphically shown in Fig. 1. In general terms, those studies have showed that increasing the lateral confining stress can improve to some extent the mechanical properties of RAC (i.e., peak axial stress, axial strain at the peak stress and elastic moduli). However, most of the explorations generally stay with only the phenomenon-based descriptions and there lacks



(a) Axisymmetric triaxial compression



(b) True triaxial compression

Fig. 1. Stress conditions of triaxial compression.

of reliable tools to quantify the behavior of RAC under triaxial load. As one of the exceptions, Folino et al. [24] successfully reformulated their previously proposed “Performance Dependent Failure Criterion” on RAC under triaxial compression based on a small range of test results. Although, the proposed model is with strong physical significance, its expressions may be a bit difficult, which is hard to be directly adopted in daily design work. He et al. [28] suggested a multi-axial failure criterion for triaxially-loaded RAC by fitting their experimental results; however, that criterion ignores the cases with RCA replacement ratio exceeding 50% (i.e., $RCA\% < 50\%$).

Based on the foregoing literature review, there are still no practical prediction methods, either in algebraic form or expressed as numerical procedures, that can be directly used to estimate the behavior of RAC under multi-axial stress states.

Nevertheless, some of the existing approaches (e.g., [30–49]) derived empirically for multi-axially loaded (or confined) NAC, as summarized in Table 1, still have the potential to be applied to RAC to solve such complex problem. At the outset, those models need to be carefully evaluated or calibrated for their extended use to RAC, which is one of the motivations of this research, and directly yields a new set of more accurate enclosed-form formulas.

In addition to examining the aforementioned conventional models, introducing Artificial Intelligence (AI) techniques into the problem at hand is also the objective of this study. Those techniques are mostly data-driven approaches which are capable of learning directly from experimental data, thus they have aroused significant interest in the past few years. A broad spectrum of computer-assisted intelligence methods, such as artificial neural networks, fuzzy logic, model tree algorithm, genetic algorithm, and gene expression programming, have been used to evaluate the effects of multi-parametric variables on the uniaxial behavior of RAC due to their accuracy and reliability [50–60]; however, when it comes to the triaxial behavior of RAC, little analogous research can be found.

To predict more rationally the triaxial behavior of RAC with AI techniques, a two-stage combined methodology is proposed in this research. First the grey correlation analysis (GCA) is conducted to determine the sensitivity of parameters that could affect the performances of RAC under multi-axial conditions. Subsequently, a traditional function-mining method—the second-order polynomial based Multivariable Nonlinear Regression (MNR), and two robust Artificial Neural Networks (ANN), i.e., the Back-Propagation (BP) based ANN and the newly-emerged hybrid Genetic Algorithm (GA) optimized ANN are applied to estimate the behavior of RAC under triaxial load. In the latter three models, their input parameters are exactly those identified by the previous GCA, thus avoiding any blind selection of influential factors.

It is noteworthy that GCA is an attractive, powerful mathematical tool for evaluating the sensitivity of independent variables to dependent variables in term of their grey correlations; that is, GCA can be used to predict the geometric proximity between different discrete sequences within a system [61]. Ranking of grey correlations derived by GCA is then utilized as the indicator for judging the importance of these parameters. Recently, Xu et al. [62,63] have used this method to successfully determine the parametric sensitivity of variables on the compressive and seismic behaviors of reinforced concrete columns manufactured using RAC. However, a literature review by the authors has indicated that there are still no relevant studies extending the use of GCA to the prediction of the triaxial behavior of RAC.

The methods presented in this paper are developed based on a comprehensive experimental database that is carefully assembled using a set of selection criteria. Significantly, this is the first study to propose practical yet accurate models for the evaluation of multi-axial behavior of RAC, also the first study that synthesizes

Table 1
Summary of empirical models for predicting peak stress and peak strain of NAC under axisymmetric triaxial load.

Mechanical property	Source	Model	Source	Model
Peak stress	Richart et al. [30]	$(\sigma_1/f'_c) = 1 + 4.1(\sigma_3/f'_c)$	Attard and Setunge [38]	$(\sigma_1/f'_c) = [1 + (\sigma_3/f'_t)]^k; \quad k = 1.25[1 + 0.062(\sigma_3/f'_c)](f'_c)^{-0.21},$ $f_{tsp}/f'_c = 0.387f'_c^{-0.37}, \quad f_t = 0.9f_{tsp}$
	Balmer [31]	$(\sigma_1/f'_c) = [1 + 9.175(\sigma_3/f'_c)]^{0.73}$	Lan and Guo [39]	$(\sigma_1/f'_c) = 1 + 6.74(\sigma_3/f'_c) - 2.03(\sigma_3/f'_c)^2$
	Chinn and Zimmerman [32]	$(\sigma_1/f'_c) = 1 + (8.2/f'_c)(\sigma_3)^{0.883}$	Ansari and Li [40]	$(\sigma_1/f'_c) = 1 + 2.45(\sigma_3/f'_c)^{0.703}$
	Ayram et al. [33]	$(\sigma_1/f'_c) = 1 + 3.7(\sigma_3/f'_c)^{0.86}$	Samaan et al. [41]	$(\sigma_1/f'_c) = 1 + 6(\sigma_3^0/f'_c)$
	Martinez et al. [34]	$(\sigma_1/f'_c) = 1 + 4(\sigma_3/f'_c)$	Li and Ansari [42]	$(\sigma_1/f'_c) = 1 + 2.4305(\sigma_3/f'_c)^{0.6376}$
	Saatcioglu and Razvi [43]	$\sigma_1 = f'_{co} + K_1 \cdot K_2 \cdot \sigma_3; \quad K_1 = 6.7(K_2 \cdot \sigma_3)^{-0.17}, \quad K_2 = 1, \quad f'_{co} = 0.85f'_c$		$\sigma_1 = f'_{co} + K_1 \cdot K_2 \cdot \sigma_3; \quad K_1 = 6.7(K_2 \cdot \sigma_3)^{-0.17}, \quad K_2 = 1, \quad f'_{co} = f_c$
	Setunge et al. [36]: Equation I	$(\sigma_1/f'_c) = [1 + 18.67(\sigma_3/f'_c)]^{0.45}$	Légeron and Paultre [44]	$(\sigma_1/f'_c) = 1 + 2.4(\sigma_3/f'_c)^{0.7}$
	Setunge et al. [36]: Equation II	$(\sigma_1/f'_c) = [1 + 14.67(\sigma_3/f'_c)]^{0.45}$	Girgin et al. [45]	$(\sigma_1/f'_c) = 1 + 4.08(\sigma_3/f'_c)^{0.83}$
	Setunge et al. [36]: Equation III	$(\sigma_1/f'_c) = [1 + 13.07(\sigma_3/f'_c)]^{0.63}$	Bohwani et al. [46]	$(\sigma_1/f'_c) = 1 + 4.352(\sigma_3/f'_c) - 2.769(\sigma_3/f'_c)^2$
	Xie et al. [37]	$(\sigma_1/f'_c) = [1 + k(\sigma_3/f'_c)]^{0.5}; \quad k = 21.2 - 0.05f'_c$	Tang [48]	$(\sigma_1/f'_c) = 1.2 + 3.4(\sigma_3/f'_c)$
Peak strain	Richart et al. [30]	$(\varepsilon_1/\varepsilon_0) = 5(\sigma_1/f'_c) - 4$	Attard and Setunge [38]	$(\varepsilon_1/\varepsilon_0) = 1 + (17 - 0.06f'_c)(\sigma_3/f'_c)$
	Ansari and Li [40]	$(\varepsilon_1/\varepsilon_0) = 1 + 15.15(\sigma_3/f'_c)$	Candappa et al. [43]	$(\varepsilon_1/\varepsilon_0) = 1 + 20(\sigma_3/f'_c)$
	Tang [48]: Equation I	$(\varepsilon_1/\varepsilon_0) = 0.68 + 8.1[\ln(\sigma_1/f'_c)]^2$	Tang [48]: Equation II	$(\varepsilon_1/\varepsilon_0) = 1.39[0.5 + (17 - 0.06f'_c)(\sigma_3/f'_c)]$
	Samani and Attard [49]	$(\varepsilon_1/\varepsilon_0) = e^k; \quad k = (2.9224 - 0.00367f'_c)(\sigma_3/f'_c)^{[0.3124+0.002f'_c]}$		

the so-far experimental outcomes to reach a further understanding of RAC under triaxial stress conditions. Ultimately, the models developed in this study would redound to transferring such a green material into reliable and cost-effective applications, thus contributing to the sustainable constructions.

2. Experimental database, existing empirical models and new design-oriented model

2.1. Construction of experimental database

An experimental test database was constructed based on an extensive perusal and collection of information in reference documents regarding the experimental tests of RAC under triaxial load [23–29]. To ensure the reliability and consistency of the database, the following selection criteria are applied to the specimens before their inclusion in the final database:

- (1) Detailed mix proportions of concrete were provided;
- (2) No pozzolanic or supplementary cementitious materials were incorporated in RAC mixes;
- (3) No chemical pre-treatments to RCA were used;
- (4) The compressive strength was experimentally obtained with cube specimens of an aspect ratio of 1.0 or cylindrical specimens of an aspect ratio of 2.0;

By subjecting these criteria, the final test database presented in **Tables A1 and A2** in Appendix is constructed, comprising 248 datasets collected from seven experimental studies—four related to axisymmetric triaxial tests as reported in **Table A1** and three on true triaxial tests as shown in **Table A2**. Specifically, the database contains a total of 193 peak stress (σ_1) results obtained from cylinder specimens, 55 peak stress (σ_1) results obtained from cube specimens, 61 elastic moduli (E_c) results from cylinder specimens, and 76 peak strain (ε_1) results from cylinder specimens.

In **Tables A1 and A2**, the following information is given for each dataset: the type and size of the specimens (i.e., D is the diameter of cylinder specimen, B is the edge-length of cube specimen, and H is the height of cylinder or cube specimen), the effective water-to-cement binder ratio (w_{eff}/c), aggregate-to-cement ratio (a/c), RCA replacement ratio ($RCA\%$), water absorption of RCA and NA (WA_{RCA} and WA_{NA} , respectively), bulk density of coarse RCA and NA ($\rho_{bd,r}$ and $\rho_{bd,n}$, respectively), apparent density of coarse RCA and NA ($\rho_{ad,r}$ and $\rho_{ad,n}$, respectively), crush index of coarse RCA and NA (Cl_{RCA} and Cl_{NA} , respectively), stress conditions (i.e., $\sigma_2:\sigma_1$, $\sigma_3:\sigma_1$ and σ_3), exposure temperature (T), uniaxial compressive strength of concrete (f'_c), uniaxial strain at f'_c (ε_0), peak stress of concrete (σ_1), elastic moduli of concrete (E_c) and peak strain (ε_1) corresponding to peak stress. Detailed information of RAC specimens in each individual study is summarized in **Table 2**.

Note that two geometry types (cylinders and cubes) were used in those tests. The aspect ratio for cubes and cylinders are 1.0 and 2.0, respectively. In addition, two different cross-sectional sizes were adopted for each geometry type: (i) for cylinders of 50 mm (labeled as C1 in **Tables A1 and A2**) or 100 mm diameter (C2); and (ii) for cubes of 100 mm (S1) or 150 mm dimension (S2). The conversion rules for translating the uniaxial compressive strengths between cubes and cylinders follow exactly the specifications in the CEB-FIP Model Code 2010 [64].

It should also be mentioned that, in **Table A1**, 100 results of axisymmetric triaxial tests by Meng et al. [26] were obtained via testing RAC specimens after exposure to high temperatures above 200 °C, while the rest in **Tables A1 and A2** were obtained at ambient temperature. Thus the exposure temperature is also deemed as a decisive parameter in this study.

Table 2
Detailed information for RAC specimens under triaxial load in the compiled database.

Source ^a	Specimen diameter, D [mm]	Specimen height, H [mm]	Lateral stress, σ_3 [MPa]	Exposure temperature, T [°C]	RCA replacement ratio, $RCA\%$	Effective water-to-cement binder ratio, w_{eff}/c	Aggregate-to-cement ratio, a/c
Yang et al. [23]	50	100	0–32	Room temperature	0–100%	0.40	2.50
Folino and Xargay [24]	100	200	0–40	Room temperature	0–100%	0.50–0.56	2.85–3.10
Chen et al. [25]	100	200	0–27	Room temperature	0–100%	0.32–0.41	1.50–2.31
Meng et al. [26]	100	200	0–20	Room temperature, and 200–500	0–100%	0.41	2.15
Source ^b	Specimen edge-length, B [mm]	Specimen height, H [mm]	Stress ratio $\sigma_3:\sigma_1$	Stress ratio $\sigma_2:\sigma_1$	RCA replacement ratio, $RCA\%$	Effective water-to-cement binder ratio, w_{eff}/c	Aggregate-to-cement ratio, a/c
He et al. [27]	150	150	0–0.1	0–1.0	30–50%	0.37–0.40	3.13–3.17
He et al. [28]	150	150	0–0.1	0–1.0	30%	0.30–0.51	2.35–4.75
Deng et al. [29]	100	100	0.1	0.25–1.0	0–100%	0.43–0.47	2.46–2.70

^a Cylinder specimens tested under uniaxial and axisymmetric triaxial loads.

^b Cubic specimens tested under uniaxial and true triaxial loads, and no exposure temperature acting on RAC specimens.

To scrutinize the beneficial effect of lateral confinement in triaxial tests of RAC specimens, Fig. 2 shows the gain in strength (σ_1/f'_c) as a function of RCA% for different ranges of σ_3 . It is clear that those gains are varied depending on RCA% as well as on σ_3 : (i) for $0 < \sigma_3 \leq 20$ MPa, increasing the RCA replacement ratio generally leads to a decrease in σ_1/f'_c ; and (ii) for $20 < \sigma_3 \leq 32$ MPa, σ_1/f'_c becomes not so sensitive to the RCA replacement ratio. This manifests that once subjected to a sufficiently high lateral confining stress σ_3 (i.e., over 20 MPa), the effect of inferior properties of RCA on the compressive strength tends to diminish.

2.2. Assessment of existing empirical models

A number of empirical models for predicting the peak stress as well as the strain at the peak stress (called peak strain hereafter) of NAC under axisymmetric triaxial load (or in so-called confined state) have been proposed in the past decades. Table 1 summarizes

typical existing empirical models [30–49], in which twenty models are suggested for the peak stress prediction while seven for the peak strain.

It should be highlighted that these models are all developed from regression analysis, during which the uniaxial unconfined compressive strength of concrete (f'_c) and the lateral stress (σ_3) are considered as the primary parameters.

The applicability of those models listed in Table 1 for the recycled aggregate concrete under axisymmetric triaxial load need to be assessed. The database described in Section 2.1 is used to assess the model performance. Fig. 3 shows the comparisons between experimental results and model predictions on the peak stress and peak strain of RAC under axisymmetric triaxial load. From the comparisons, it can be found that: (i) for the peak stress (Fig. 3a), the ratio of the predicted peak stress-to-the experimental one is equal to 0.851, significantly less than a unit, indicating the over-conservatism of those predictive models; (ii) for the peak

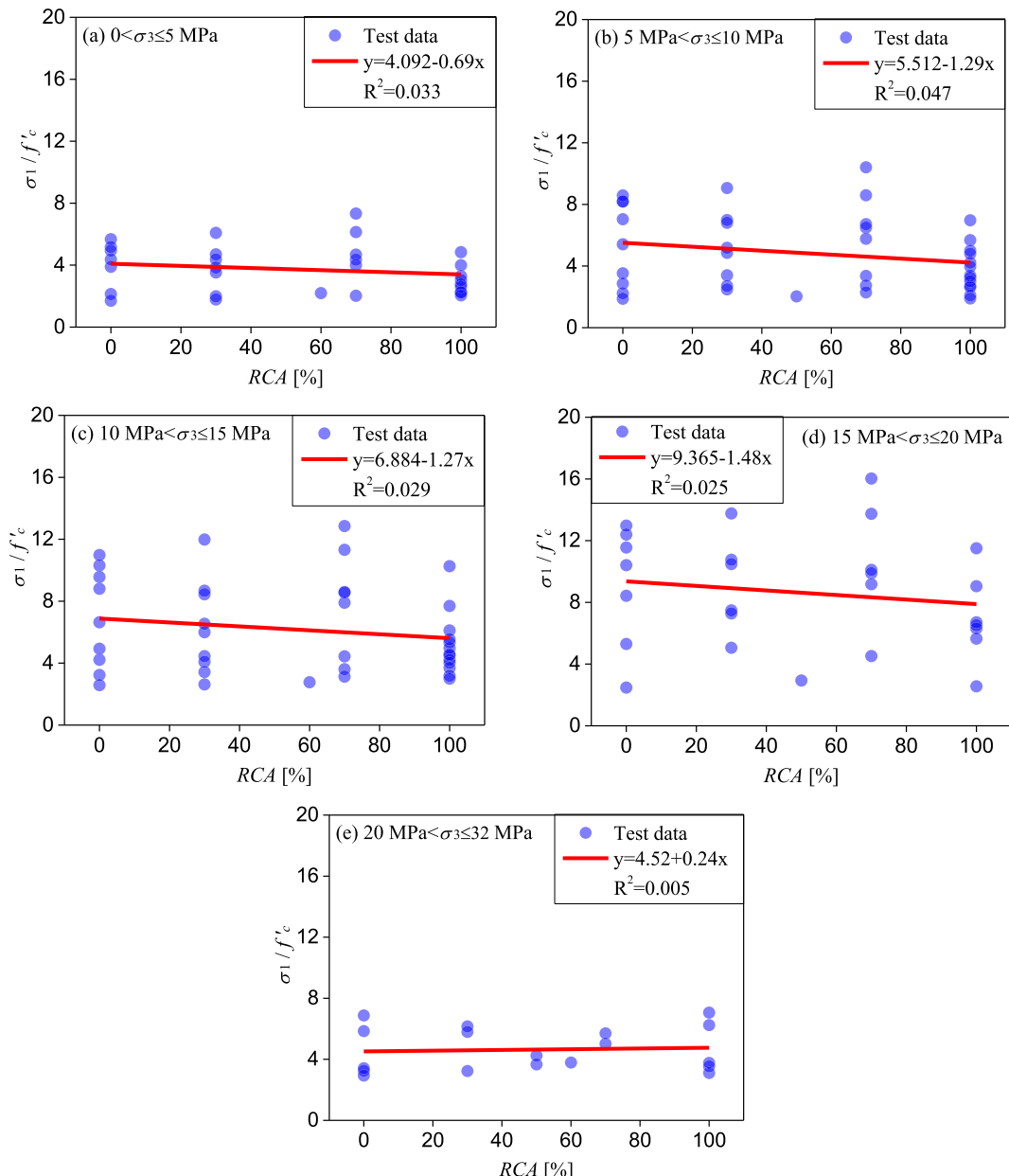


Fig. 2. Strength enhancements for RAC under triaxial loads.

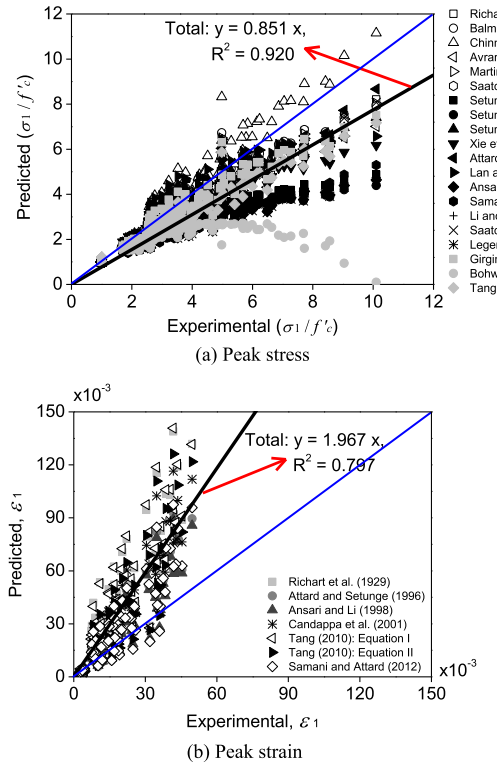


Fig. 3. Predictions using existing empirical models for the peak stress and peak strain of RAC under axisymmetric triaxial load.

strain (Fig. 3b), even worse shoot is exhibited: the ratio of the predicted peak strain-to-the experimental one is as high as 1.967, signifying an overall failure in terms of prediction accuracy.

The limitation of accuracy with regard to those existing empirical models for the case of RAC may be explained by two factors: (i) first, the effect of RCA was entirely not considered when developing those models as they were developed solely for and calibrated only using the test results of NA-based concrete (specimens). For example, the incorporation of RCA generally induces much greater values of peak strain in comparison with that of NAC. Thus the prediction performance on the peak strain of RAC are markedly poorer than those on peak stress; (ii) often, RAC specimens have larger scatters than their NAC counterparts, particularly on the deformation characteristics. In a word, the prediction errors of the existing empirical models underline the need of new models for predicting the responses of RAC under axisymmetric triaxial loading conditions.

2.3. New empirical model for predicting axisymmetric triaxial behavior of RAC

As noted from Table 1, the majority of the collected models for NAC under axisymmetric triaxial load have quite similar form as they are generally adapted from that established by Richart et al. [30]. In this paper, Richart et al. [30]'s model is also used as the baseline to develop a new set of empirical formulas to predict the behavior of RAC under axisymmetric triaxial conditions. Through fitting the data points of the database compiled previously (see Figs. 4 and 5), the following equations are suggested:

(1) for the peak stress of RAC:

$$\sigma_1/f'_c = \begin{cases} 1 + 7.08\ln^{(\lambda+1)} & T = 20^\circ\text{C} \\ 1 + 7.26\ln^{(\lambda+1)} & 200^\circ\text{C} < T \leq 500^\circ\text{C} \end{cases} \quad (1)$$

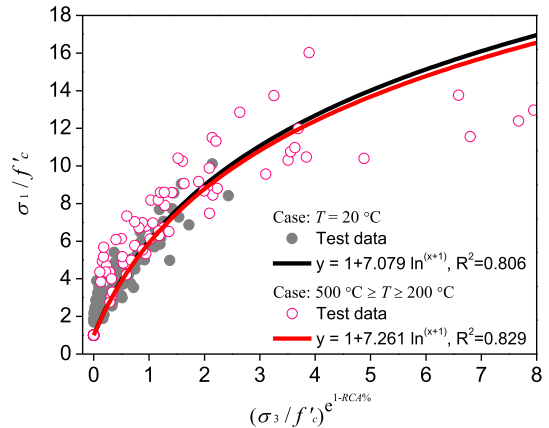


Fig. 4. Developed empirical model for predicting the peak stress of RAC under axisymmetric triaxial load.

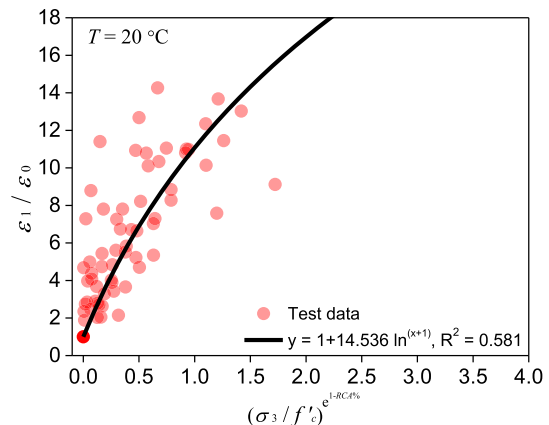


Fig. 5. Developed empirical model for predicting the peak strain of RAC under axisymmetric triaxial load.

$$\lambda = (\sigma_3/f'_c)^k, k = e^{1-RCA\%}$$

(2) for the peak strain of RAC:

$$\epsilon_1/\epsilon_0 = 1 + 14.54\ln^{(\lambda+1)} \quad T = 20^\circ\text{C} \quad (2)$$

$$\lambda = (\sigma_3/f'_c)^k, k = e^{1-RCA\%}$$

where ϵ_0 is the uniaxial peak strain at the unconfined peak stress f'_c of unconfined RAC; note that f'_c can be further calculated according to Xu et al. [60] in which the RCA% and the w/c ratio are taken into account (i.e., the cylindrical compressive strength of RAC $f'_c = \frac{28.8 - 5.7RCA\%^{1.7}}{(w/c)^{0.63}}$) and developed based on an extensive database.

Note that when modeling the triaxial behavior of the specimens subjected to high temperature, the companion material properties of the concrete (i.e., unconfined compressive strength) subjected to the same temperature aiming to avoid the effect of degradation of concrete material under high temperature should be adopted. This leads to the development of the empirical models only reflecting the mechanism governing the performance of the concrete under triaxial load.

As can be seen from Figs. 4 and 5, the new empirical model correlates much better with the experimental results than the average performance of the previous empirical models. Hence, they can be used as reliable basis in quick estimation of the performance of RAC under axisymmetric triaxial load. For more accurate predictions, the following sections provide more complex alternatives.

3. Grey correlation analysis

3.1. The principle of grey correlation theory

In this study, grey correlation theory was used to determine the parametric sensitivity of the behavior of RAC under triaxial load. The peak stress (σ_1), peak strain (ϵ_1), and elastic moduli (E_c) are determined as the reference matrix, $\mathbf{X}_0(j)$, where $j = 1, 2, \dots, n$. The key experimental variables, including RCA%, concrete mixture proportions (i.e., a/c and w_{eff}/c), exposure temperature (T), and stress conditions (i.e., $\sigma_2:\sigma_1$, $\sigma_3:\sigma_1$ and σ_3) are selected as the comparative matrix, $\mathbf{X}_i(j)$, where $i = 1, 2, \dots, m$. The following sets of equations are used for constructing of the reference matrix and the comparative matrix according to the grey correlation theory:

$$\begin{aligned} \mathbf{X}_0 &= \mathbf{X}_0(1), \mathbf{X}_0(2), \dots, \mathbf{X}_0(n) \\ \mathbf{X}_1 &= \mathbf{X}_1(1), \mathbf{X}_1(2), \dots, \mathbf{X}_1(n) \\ &\dots \\ \mathbf{X}_m &= \mathbf{X}_m(1), \mathbf{X}_m(2), \dots, \mathbf{X}_m(n) \end{aligned} \quad (3)$$

In order to reduce the numerical fluctuation, a normalization process can be conducted:

$$x_i(j) = \frac{\mathbf{X}_i(j)}{\sum_{i=1}^n \mathbf{X}_i(j)} \quad (4)$$

The grey correlation coefficient ξ_i can thus be obtained:

$$\xi_i[\mathbf{x}_0(j), \mathbf{x}_i(j)] = \left| \frac{\min_{i=1,n} \min_{j=1,m} \Delta_i(j) + \rho \max_{i=1,n} \max_{j=1,m} \Delta_i(j)}{\Delta_i + \rho \max_{i=1,n} \max_{j=1,m} \Delta_i(j)} \right| \quad (5)$$

$$\Delta_i(j) = |\mathbf{x}_0(j) - \mathbf{x}_i(j)| \quad (6)$$

$$\min_{i=1,n} \min_{j=1,m} \Delta_i(j) = \max_i (\max_j |\mathbf{x}_0(j) - \mathbf{x}_i(j)|) \quad (7)$$

$$\max_{i=1,n} \max_{j=1,m} \Delta_i(j) = \min_i (\min_j |\mathbf{x}_0(j) - \mathbf{x}_i(j)|) \quad (8)$$

where $0 \leq \rho \leq 1$, and its frequently-used value is 0.5 [61].

In the GCA, grey correlation factor (λ) can be used to measure the degree of correlation between the reference matrix and the comparative matrix:

$$\lambda = \frac{1}{n} \sum_{i=1}^n \xi_i[\mathbf{x}_0(j), \mathbf{x}_i(j)] \leq 1.0 \quad (9)$$

It is worth noting that the value of λ approaching the unity indicates a very strong correlation between the independent variables and the dependent variables; when λ is over 0.7, the correlation sensitivity is still prominent; when λ is less than 0.5, the correlation is weak and indicates the selected parameter has a less significant effect on the target property [61].

3.2. Parametric sensitivity evaluation on the behavior of RAC under triaxial load

3.2.1. Peak stress of RAC

Fig. 6a and b show the ranks of the sensitivity of the key parameters on the peak stress of RAC under axisymmetric or true triaxial load, respectively. It can be observed from the average ranking of the grey correlation factor (λ) illustrated in Fig. 6a and b that: (1) for axisymmetric triaxial tests, $T > \sigma_3 > a/c > w_{eff}/c > RCA\%$; (2) for true triaxial tests, $a/c \approx w_{eff}/c \approx \sigma_2:\sigma_1 > \sigma_3:\sigma_1 > RCA\%$. Evidently, the temperature exposure has the largest sensitivity effect the peak stress of RAC under triaxial load (for the case of true triaxial load the relevant test data is absent up till now, but this conclusion

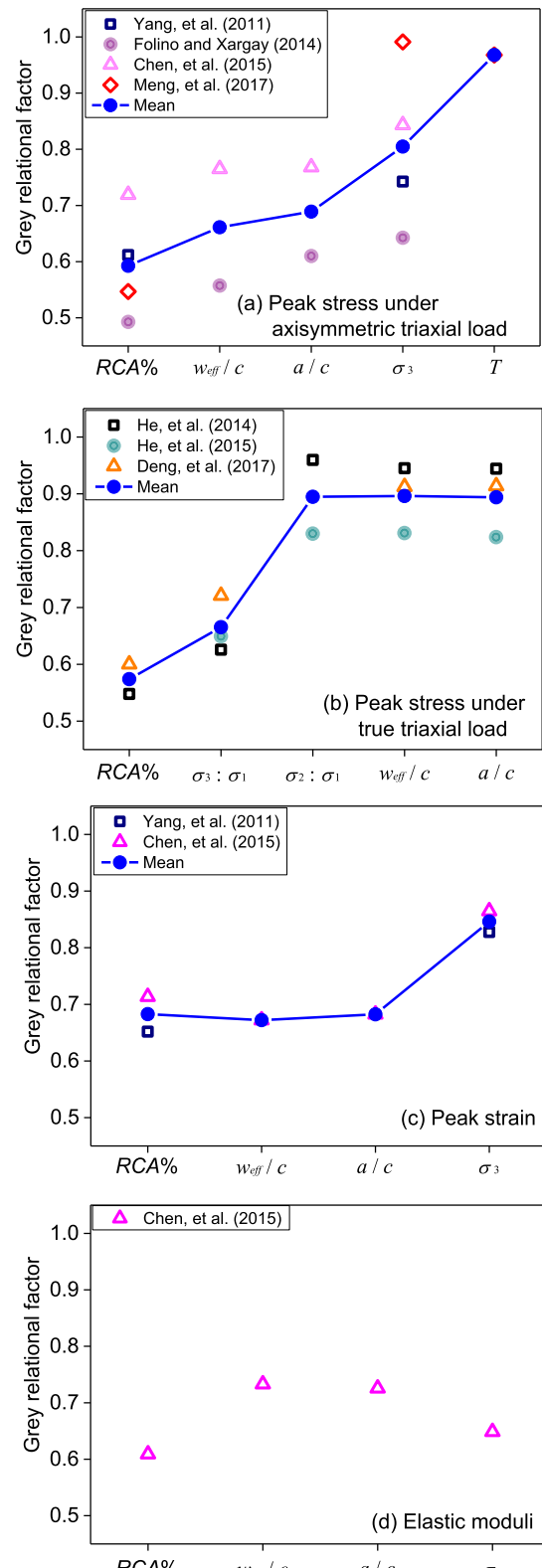


Fig. 6. Parametric sensitivity of key variables on the behavior of RAC.

should hold due to the significant deterioration of concrete materials after thermal exposure [62,63].

Through the GCA, the lateral stress (σ_3) for axisymmetric triaxial tests and the ratio of larger lateral-to-axial stress ($\sigma_2:\sigma_1$) for true triaxial tests are identified as two parameters that have strong influence on the peak stress of RAC and their sensitivities are com-

parable. This is attributed to the fact that the confinement imposed by the lateral stress restrains the dilatation of RAC and hence increases the first principal stress σ_1 [64,65].

It is worth noting that the sensitivity effect of the ratio of smaller lateral-to-axial stress (i.e., $\sigma_3:\sigma_1$ in true triaxial tests) on the peak stress of RAC is much less influential than that of the ratio of larger lateral-to-axial stress (i.e., $\sigma_2:\sigma_1$) (see Fig. 6b). Comparatively, for the axisymmetric case, the failure pattern of specimens is dominated solely by the level of σ_3 uniformly imposed on specimens. This is illustrated in Fig. 1a, where the failure pattern of RAC specimen changes from compression-shear failure to localized horizontal crushing with an increase of σ_3 . On the other hand, for the true triaxial load, the unevenly distributed lateral confining stresses (i.e., σ_3 and σ_2) induce more asymmetric failure, where the larger lateral stress σ_2 exerts greater effect compared to the smaller lateral stress σ_3 . The typical failure modes of RAC in this case with different stress ratios are shown in Fig. 1b.

From Fig. 6a and b, it is also evident that, in both axisymmetric and true triaxial tests, the significance of RCA% is moderate in general, with an average grey correlation factor (λ) of about 0.58. The effective water-to-cement binder ratio (w_{eff}/c) and the aggregate-to-cement ratio (a/c), both of which are intimately related to the mechanical properties of RAC (e.g., [50,66]), affect the peak stress of RAC under true triaxial load significantly (with the mean of λ near to 0.9), whereas under axisymmetric triaxial load those two parameters have a less appreciable effect (with the mean of $\lambda < 0.7$ but > 0.6). This discrepancy can be attributed that in the case of true trial load the quality of RAC (represented by w_{eff}/c and a/c) determines what level of peak stress σ_1 can be achieved, while under axisymmetric triaxial load the effect of the mechanical properties of RAC attenuate due to the more localized failure compared to the former case.

3.2.2. Peak strain of RAC

Fig. 6c shows the sensitivity effect of the key parameters on the peak strain of RAC under axisymmetric triaxial load. The average ranking of the grey correlation factor (λ) is: $\sigma_3 > RCA\% > a/c > w_{eff}/c$. Based on the calculated λ , the lateral stress has the largest sensitivity (λ is approximately 0.84) on the peak strain of RAC, indicating that the confinement effect provided by the lateral stress strongly affects the lateral dilatation of concrete as well as the first principal strain, consistent with the observations by Imran and Pantazopoulou [67] and Pu et al. [68]. Meanwhile, the effective water-to-cement binder ratio, aggregate-to-cement ratio and RCA replacement ratio, which determine the mechanical properties of the material, exhibit almost the same sensitivity effect on the peak strain of RAC.

3.2.3. Elastic moduli of RAC

Fig. 6d shows the sensitivity effect of the key parameters on the elastic moduli of RAC under axisymmetric triaxial load. The ranking of the grey correlation factor (λ) is: $w_{eff}/c > a/c > \sigma_3 > RCA\%$. In this case, the effects of aggregate-to-cement ratio and the effective water-to-cement binder ratio are nearly identical (λ is about 0.74), which are the two principal parameters determining the elastic moduli of RAC. The explanation of this fact is that the stiffness of aggregate and mortar greatly affects the elastic moduli of concrete [69,70]. Owing to this reason, the effect of both lateral stress and RCA replacement ratio on the elastic moduli of RAC is generally moderate (see Fig. 6d).

3.2.4. Summary of influential factors on the behavior of RAC under triaxial load

From the aforementioned parametric sensitivity evaluation with GCA, it can be concluded that the behavior of RAC under triaxial load depend mainly on the exposure temperature, the

magnitude of lateral stress, and the mechanical properties of RAC which are strongly correlated with its mixture proportions (i.e., effective water-to-cement binder ratio and aggregate-to-cement ratio). Those factors are then selected as the primary input parameters used for the later MNR and AI modeling.

As for the RCA replacement ratio concerned, despite its less notable effect than the above-mentioned parameters, the average grey correlation factor (λ) of RCA% for all the mechanical properties of RAC is close to 0.6, proclaiming a nontrivial impact. In addition, as widely reported in existing studies on RAC (e.g., [71–79]), the effect of RCA replacement ratio should not be neglected in assessing the performance of the corresponding concrete products as it is truly a controlling parameter and provides a physical meaning for the associated prediction models. On these accounts, the RCA replacement ratio is regarded as a factor and the weight of its effect will be properly reflected in the following modeling approaches.

4. Prediction of the triaxial behavior of RAC using multivariable regression and neural networks

4.1. Multiple nonlinear regression

Unlike the NA-based concrete, the characteristics of RCA and the critical parameters with a wide varying range in manufacturing RAC lead to a large variation and uncertainty in the prediction of the behavior of RAC under triaxial load when employing the empirical models developed for the behavior of NAC. The modified empirical model presented previously provides a good predictor to improve the accuracy of estimating the behavior of RAC under triaxial load. In order to achieve more favorable results, the Multiple Nonlinear Regression (MNR) method is utilized herein. The principle of MNR is based on the approximation theory using a second-order polynomial initially proposed by Scheffé [80]. The mathematical form of the polynomial is assumed as:

$$y = \sum_{i=1}^n \beta_i x_i + \sum_{i=1}^{n-1} \sum_{j=i+1}^n \beta_{ij} x_i x_j + \varepsilon \quad (10)$$

where y represents the dependent variable (i.e., σ_1 , ε_1 and E_c) of the triaxial response; x is the independent variable; ε denotes the normally distributed error; β_i and β_{ij} are the proportion coefficients of the first- and the second-order polynomials, respectively. Note that the coefficients of β_i and β_{ij} are needed to be determined via the nonlinear regression analysis.

4.2. Back-propagation based artificial neural network

Inspired by the biological nervous system, Artificial Neural Network (ANN) is one of the information analysis paradigms that can be utilized as powerful computational tools [81,82]. Concretely, an ANN is a dynamic function approximator that establishes the mapping between inputs and outputs, thereupon capturing complex interactions between different variables. In an ANN, a large number of artificial processing units, known as neurons, are arranged in layers (input, hidden, and output layers), which in turn are highly inter-connected. The number of neurons per layer defines the architecture of an ANN, as shown in Fig. 7.

There are generally two phases for the construction and application of an ANN: the training phase and the testing phase. In the training phase, inputs (i.e., the training data) are fed into the network to pass through the neurons multiplied by the connection weights, generating a level of activity for each neuron. This process is advanced following a certain learning rule. After converged, the trained network can then be generalized (applied) to the testing phase.

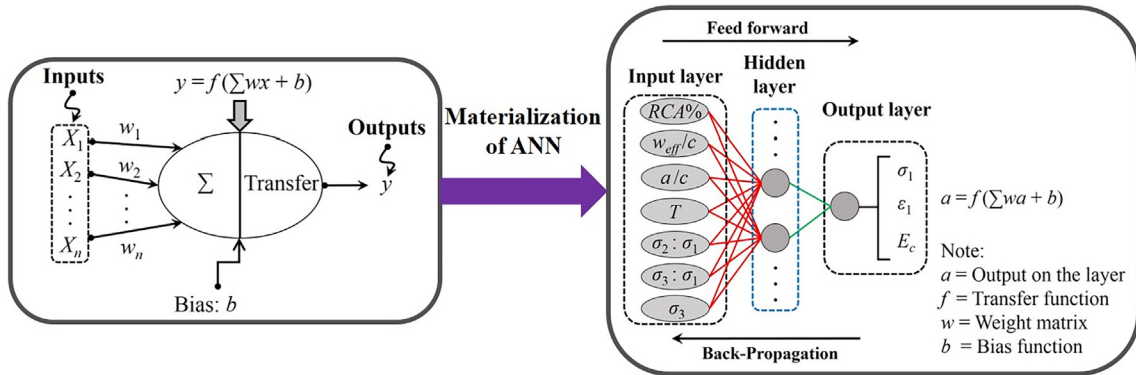


Fig. 7. Structure of artificial neuron and BP-ANN.

Among the wide variety of ANNs, the Back-Propagation (BP) neural network has been recognized as the commonly-used one which was initially developed in mid-1980s [83,84]. In the BP-ANN, errors between the computed values from the network and the target values can be backward propagated and hence be reduced by updating the weights and biases; this is essentially an error correction process. As a ripe algorithm, the BP-ANN is characterized by the simplicity and efficiency, thus has been widely used in simulating the performance of engineering materials since 1989 (e.g., [85–89]).

Generally, the BP-ANN used in this study contains five essential components: (i) input layer; (ii) weight index (w_i); (iii) sum function; (iv) transfer function; and (v) output layer. As identified by the GCA conducted previously, the RCA replacement ratio ($RCA\%$), effective water-to-cement binder ratio (w_{eff}/c), aggregate-to-cement ratio (a/c), lateral stresses conditions (i.e., $\sigma_2 : \sigma_1$, $\sigma_3 : \sigma_1$

and σ_3) and exposure temperature (T) are selected to form the input vector for the BP-ANN models; and meanwhile, the mechanical properties of RAC (i.e., peak stress, peak strain, and elastic moduli) are assembled to be the output vector (see Fig. 7). Note that it has been proved that the performance improvements by adding additional hidden layers are minor or even causes negative effect on the model performance; thus only one hidden layer is chosen here. Besides, since there is still no commonly accepted optimal method to determine the number of neurons in the hidden layer, a trial and error approach is adopted—the design of the network architecture starts with fewer hidden neurons, and then the number of hidden neurons is adjusted. Consequently, 14 neurons are used to constitute the hidden layer. The network architecture constructed is illustrated in Fig. 7.

The transfer function $f(\bullet)$ is the sum of the weighted inputs ($\sum w_i X_i$) and the bias (b), simulating the firing rate of the neuron

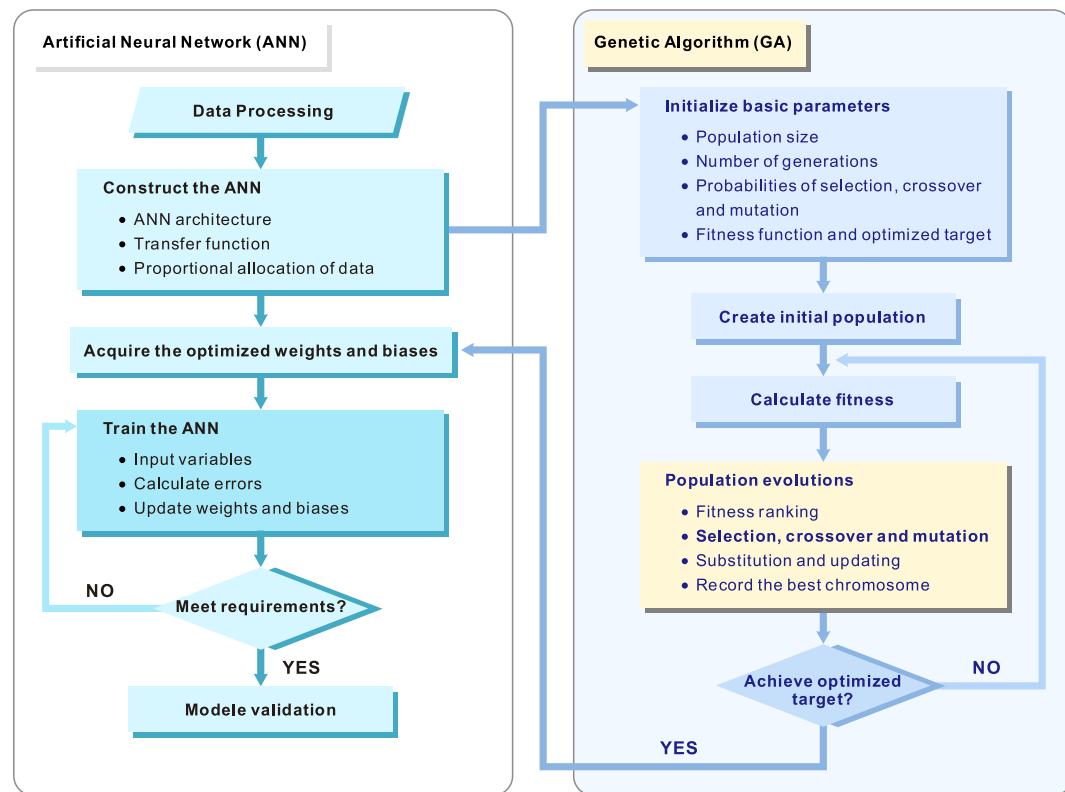


Fig. 8. Flowchart of hybrid BP-ANN optimized with GA.

Table 3

Regression coefficients in Eq. (10).

Item	Coefficient	Equation for axisymmetric σ_1^a	Equation for true σ_1^b	Equation for axisymmetric ε_1^a	Equation for axisymmetric E_c^a
1	Constant	323.794	380.990	-0.016	13.054
x_1	β_1	-138.812	-4.676	0.043	-4.773
x_2	β_2	-1279.415	427.360	0	0
x_3	β_3	21.790	57.825	0	-3.275
x_4	β_4	9.776	615.329	0	0
x_5	β_5	0	-297.087	-0.222	0
x_1x_2	β_{12}	665.792	5.134	0.019	2.791
x_1x_3	β_{13}	-56.377	-0.072	0	-0.078
x_1x_4	β_{14}	-0.544	-9.515	0	0
x_1x_5	β_{15}	-0.029	3.100	0	0
x_2x_3	β_{23}	190.857	88.342	0	0
x_2x_4	β_{24}	-9.941	4146.614	0.033	0
x_2x_5	β_{25}	0	-501.833	0.006	0
x_3x_4	β_{34}	-0.366	-376.951	-0.003	-0.118
x_3x_5	β_{35}	0.005	30.955	-0.001	0
x_4x_5	β_{45}	0.001	236.554	0	0.030

^a $x_1 = r$, $x_2 = W_{eff}/C$, $x_3 = a/C$, $x_4 = \sigma_3$, $x_5 = T$.^b $x_1 = r$, $x_2 = \sigma_2 : \sigma_1$, $x_3 = \sigma_3 : \sigma_1$, $x_4 = W_{eff}/C$, $x_5 = a/C$.**Table 4**

Parameter initializations for GA.

Parameters	Values
Population size	20
Maximum number of generations	500
Selection probability	0.9
Crossover probability	0.8
Mutation probability	0.02

to axon in the biological brain. Based on the feed-forward and the back-propagation processes, the outputs can be obtained as a function of the sum of the weighted inputs and the bias:

$$f(\text{out}_j) = \frac{1}{1 + e^{\sum w_{ij}x_i + b}} \quad (11)$$

where w_{ij} is the weight index from the lower-layer neuron i to the upper-layer neuron j ; x_i is the output of the neuron i .

4.3. Hybrid genetic algorithm-artificial neural network

As mentioned before, the incorporation of BP algorithm in the ANN modeling aims only to reduce the systematic prediction

errors. BP is known as a local search approach making use of gradient descent to update the weights and biases of the ANN. However, due to the random initialization of weights and biases, the BP-ANN could be trapped in local optima and the global optimum may not be found [90].

To remedy this, several studies have proposed to combine the BP-ANN approach with the genetic algorithms (GA) to improve the convergence to global optimum [91–93]. Those investigations indicate that GA can be harnessed to assist the training of BP-ANN so as to improve the prediction accuracy of the neural system. Therefore, the feasibility of using a hybrid genetic algorithm–artificial neural network (GA-ANN) for predicting the triaxial behavior of RAC is explored in this study.

Specifically, GA is gradient free global optimization and search technique inspired by the Darwin's natural selection and evolution theory. It has the capability to find the global optima through stochastic searching in a large solution domain. The general form GA is composed of three major processes: selection, crossover, and mutation. The mathematical background of GA can be easily found from many references (e.g., [94,95]) and is not discussed herein in detail.

Table 5

Summary of performance of BP-ANN.

Scenario	Max. and min. of exp. ^a	Max. and min. of pred.	SD of exp. ^b	SD of pred.	COV of exp. ^c	COV of pred.	R ²	MAE	MSE	RMSE	MAPE
(1) Peak stress under axisymmetric triaxial load [MPa]											
Train	219.04 (7.31)	224.98 (7.74)	40.38	40.07	0.516	0.511	0.982	4.228	29.448	5.427	0.078
Test	148.39 (10.65)	152.67 (7.51)	36.74	35.83	0.499	0.500	0.971	5.374	41.321	6.428	0.111
(2) Peak stress under true triaxial load [MPa]											
Train	280.23 (15.5)	275.63 (12.97)	81.14	81.01	0.602	0.597	0.968	7.175	225.602	15.020	0.067
Test	217.7 (20.27)	221.36 (12.65)	61.89	63.54	0.629	0.644	0.971	6.082	70.174	8.377	0.130
(3) Peak strain under axisymmetric triaxial compression [10^{-3}]											
Train	49.64 (2.18)	47.83 (2.26)	13.17	12.89	0.685	0.661	0.946	2.115	8.990	2.968	0.147
Test	38.36 (2.40)	36.85 (3.01)	10.99	10.45	0.560	0.491	0.891	2.627	11.867	3.245	0.163
(4) Elastic moduli under axisymmetric triaxial compression [GPa]											
Train	17.71 (4.60)	16.29 (5.69)	3.49	2.48	0.351	0.249	0.018	1.886	6.277	2.485	0.203
Test	12.57 (4.60)	15.31 (1.86)	2.33	3.36	0.279	0.401	0.558	1.769	4.985	2.233	0.317

^a The number outside the parenthesis is the maximum value, inside the minimum value.^b SD is the abbreviation of the standard deviation.^c COV is the abbreviation of the coefficient of variation.

In this study, GA is applied to optimize the evolution of weights and biases of the BP-ANN. The flowchart is shown in Fig. 8. The information exchange between the BP-ANN and GA is implemented through encoding and decoding the so-called chromosome on the GA side. After achieving optimal weights and biases, the ANN model is then trained using the BP algorithm, adopting just the same architecture described in Fig. 7.

4.4. Model implementation, validation and result discussion

The MNR and the two neural network models (i.e., BP-ANN and GA-ANN) are all implemented on the Matlab platform [96,97]. In the GA-ANN modeling, the key parameters such as the probabilities of selection, crossover, and mutation are initialized as those listed in Table 4.

Table 6
Summary of performance of GA-ANN.

Scenario	Max. and min. of exp. ^a	Max. and min. of pred.	SD of exp. ^b	SD of pred.	COV of exp. ^c	COV of pred.	R ²	MAE	MSE	RMSE	MAPE
(1) Peak stress under axisymmetric triaxial load [MPa]											
Train	219.04 (7.31)	218.57 (8.16)	40.38	40.31	0.516	0.513	0.987	3.505	21.895	4.679	0.069
Test	148.39 (10.65)	153.15 (10.87)	36.74	36.51	0.499	0.510	0.990	2.991	13.221	3.636	0.065
(2) Peak stress under true triaxial load [MPa]											
Train	280.23 (15.5)	276.81 (19.54)	78.86	79.51	0.633	0.652	0.987	5.633	84.008	9.156	0.075
Test	273.8 (32.19)	262.66 (32.13)	78.53	72.82	0.561	0.527	0.983	7.922	93.517	9.310	0.066
(3) Peak strain under axisymmetric triaxial compression [10^{-3}]											
Train	49.64 (2.18)	50.81 (2.51)	13.17	12.39	0.685	0.623	0.932	2.413	10.214	3.196	0.123
Test	38.36 (2.40)	39.85 (3.51)	10.99	11.23	0.560	0.540	0.886	3.145	18.104	4.254	0.328
(4) Elastic moduli under axisymmetric triaxial compression [GPa]											
Train	16.47 (4.60)	16.57 (4.19)	3.42	3.09	0.352	0.331	0.490	1.406	5.310	2.304	0.146
Test	17.71 (6.29)	14.10 (2.65)	2.95	2.92	0.305	0.384	0.445	2.224	7.872	2.806	0.295

^a The number outside the parenthesis is the maximum value, inside the minimum value.

^b SD is the abbreviation of the standard deviation.

^c COV is the abbreviation of the coefficient of variation.

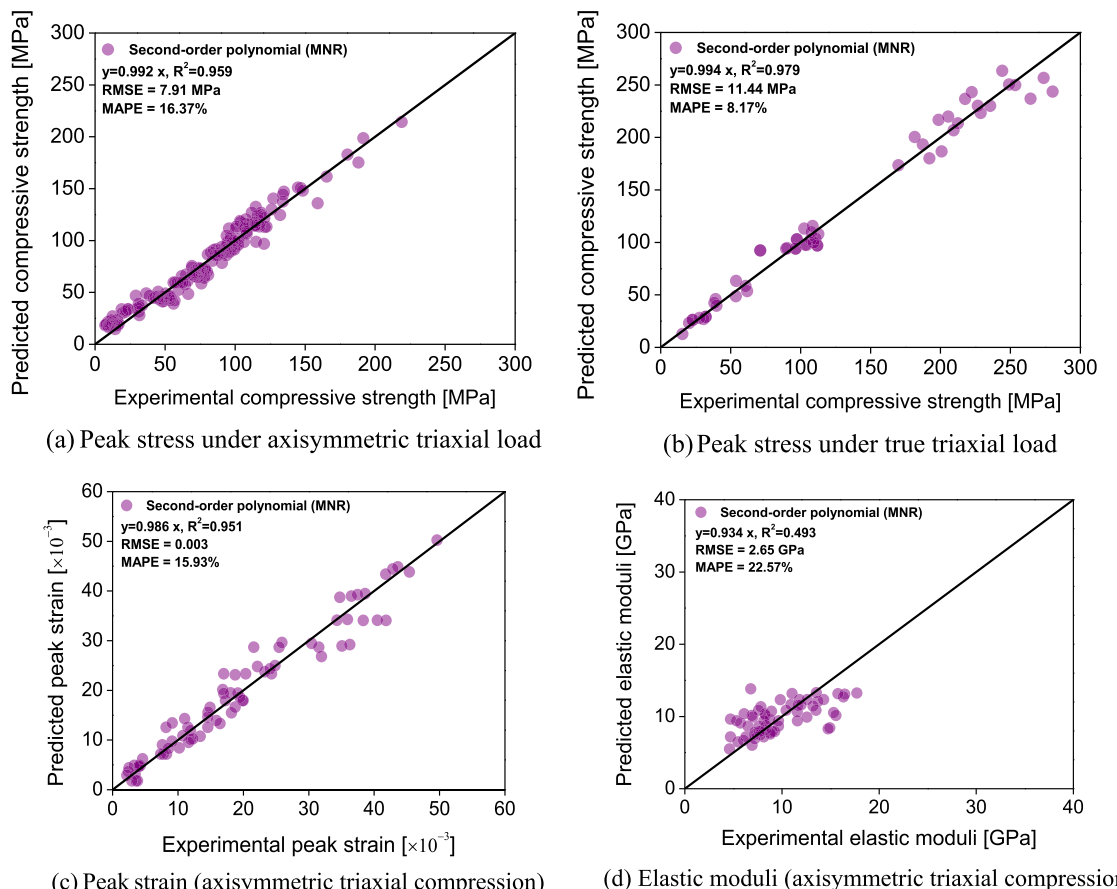


Fig. 9. MNR predictions on the behavior of RAC under triaxial loads.

Before fed into the networks, the raw data in **Tables A1 and A2** are normalized between 0 and 1 to avoid numerical difficulties or the undesirable conditions in which attributes with greater ranges dominate those with smaller ranges [98]; the following normalization rule is applied for each data:

$$X_{i,\text{norm}} = \frac{X_i - X_{\min}}{X_{\max} - X_{\min}} \quad (12)$$

where $X_{i,\text{norm}}$ and X_i are the normalized and the original input variable, respectively; X_{\max} and X_{\min} are the maximum and minimum values of the input variable, respectively. Note that if X_{\max} equals to X_{\min} , the above normalization process should be omitted.

For database partitioning, both the BP-ANN and GA-ANN models are trained using 80% of the total database, which is indiscriminately selected to avoid any bias [99,100]. The remaining 20% is used for testing the generalization capability of the two types of neural networks.

To measure the prediction accuracy, descriptive statistics including coefficient of determination (R^2), Mean Average Error (MAE), Mean Square Error (MSE), Root Mean Square Error (RMSE), and Mean Absolute Percentage Error (MAPE) are used in this study. The R^2 is an often used indicator that measures the degree of association between measured and predicted values. In addition, the RMSE gives a relatively high weight to large errors since the errors are squared before they are averaged, while the MAPE allows a mean measure of the prediction accuracy. Generally, higher R^2 and lower errors indicate good model performance. The MAE, MSE, RMSE and MAPE can be obtained using the following formulas:

$$\begin{aligned} \text{MAE} &= \frac{\sum_{i=1}^n |\text{Mod}_i - \text{Exp}_i|}{n}; \text{MSE} = \frac{\sum_{i=1}^n (\text{Mod}_i - \text{Exp}_i)^2}{n} \\ \text{RMSE} &= \sqrt{\frac{\sum_{i=1}^n (\text{Mod}_i - \text{Exp}_i)^2}{n}}; \text{MAPE} = \frac{1}{n} \sum_{i=1}^n \frac{|\text{Mod}_i - \text{Exp}_i| \times 100\%}{\text{Exp}_i} \end{aligned} \quad (13)$$

where Mod_i and Exp_i are the predicted output matrix and the real output matrix, respectively; and n is the total number of the training and testing processes.

With the above appraisal indices, the performance of the MNR method and the two developed neural networks can be readily assessed. For the convenience of comparison, the performances of the BP-ANN and GA-ANN in terms of those indices and the other often-used statistical indicators (such as SD and COV) are summarized in **Tables 5 and 6**, respectively.

For the MNR method, the proportion coefficients listed in **Table 3** are the most important elements to form the mathematical equation (i.e., Eq. (10)) for predicting the triaxial behavior of RAC. A comparison between the MNR predictions and the experimental data is plotted in **Fig. 9(a)-(d)**. It can be seen that this approach achieves improved prediction accuracy compared to the existing empirical models. Overall, the peak stress under axisymmetric triaxial load can be well reproduced by the MNR, with the $R^2 = 0.959$. The accuracy for capturing the peak strain under axisymmetric triaxial conditions is also substantially improved using the MNR (**Fig. 9(c)**), increasing the value of R^2 from 0.797 (**Fig. 3(b)**) to 0.951 (**Fig. 9(c)**). Moreover, the MNR predict with reasonable accuracy the elastic moduli, though inferior than modeling other triaxial properties of RAC. This may be caused by the inherent scatter of the measured deformation characteristics of concrete materials.

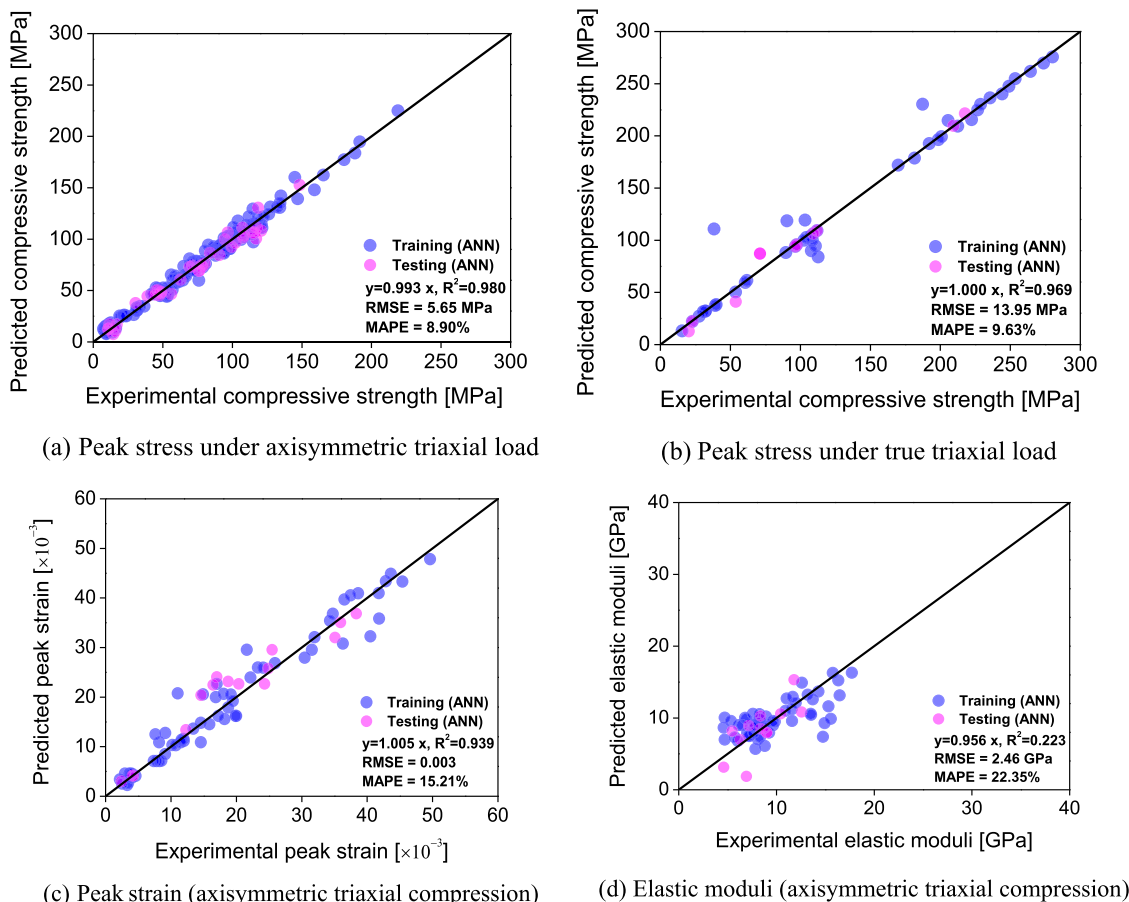


Fig. 10. BP-ANN predictions on the behavior of RAC under triaxial loads.

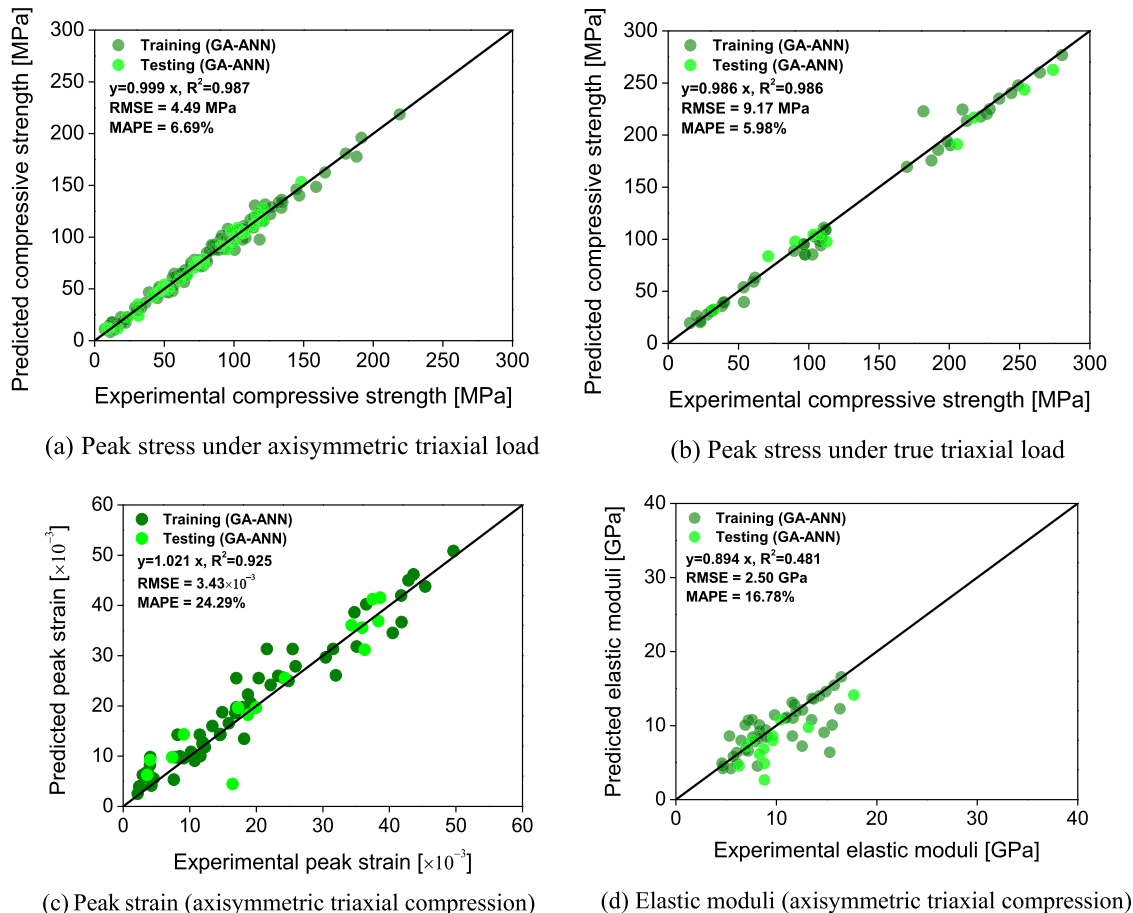


Fig. 11. GA-ANN predictions on the behavior of RAC under triaxial loads.

Fig. 10(a)–(d) shows the plots of the training and testing results against the experimental measurements using the BP-ANN. The indices in those plots are calculated for the whole data sets (i.e., including both training and testing data). Again, the BP-ANN shows a clear superiority in comparison with the existing empirical models in both data fitting and estimation capabilities. The values of R^2 for the peak stress estimation using the MNR and BP-ANN are generally comparable. For instance, under the specific axisymmetric triaxial load, the R^2 of the BP-ANN and the MNR prediction are 0.980 and 0.959, respectively.

Fig. 11(a)–(d) demonstrates the predictions of the behavior of RAC under triaxial load using the GA-ANN. It is observed that on the estimation of the peak strength, the performance of GA-ANN is slightly enhanced with regard to that of the BP-ANN, particularly for the case of true triaxial load scenario. In specific terms, both of the two values of R^2 for the GA-ANN in predicting the peak stress under axisymmetric and true axial loads are close to 0.990, being the highest among the proposed models, which indicates that only about 1.0% of the total variations are not explained by the GA-ANN for the overall data set. The superior performance of the GA-ANN can be attributed to the optimal weights and biases in neural network with the aid of the GA approach. As is shown in **Fig. 11(c)**, the GA-ANN adequately predicts the peak strain of RAC under triaxial load. However, on estimating the elastic moduli (**Fig. 11(d)**), a similar inferior performance is exhibited for the GA-ANN to those observed in the MNR and the BP-ANN, indicating that more accurate test data and refined models are needed.

To sum up, the applications of the four suggested models (i.e., the empirical design-oriented model, the MNR model, the BP-ANN and GA-ANN models) on predicting the triaxial behavior of

RAC should be very useful. In point of view of practitioners, the developed design-oriented models can serve as a reliable and efficient base with acceptable accuracy. The MNR model developed with a satisfactory performance is also easy-to-implement to estimate the performance of RAC under triaxial load with the presence of its mathematic forms. Nevertheless, this surely does not devalue the two neural networks developed, which can be easily realized and provide reliable alternatives that reflect complicated interrelationships between the triaxial behavior of RAC and the important design factors.

5. Conclusions

In the present investigation, based on the database constructed for the behavior of RAC under triaxial load, the performance of typical existing empirical models collected from the literature is evaluated. The undesirable accuracies of those models motivate to develop four different types of models, including the design-oriented model, the MNR, the BP-ANN and the GA-ANN. Before developing new models, a grey correlation analysis is conducted, which is helpful to check the sensitivity of key parameters that affect the triaxial behavior of RAC. Based on the results presented herein, the following conclusions can be drawn:

- (1) The confinement effect is beneficial to compensating the detrimental effect of incorporating RCA in new concrete. In general, with a sufficiently high lateral confining stress σ_3 (i.e., $\sigma_3 > 20$ MPa), the negative effect of inferior properties of RCA on the compressive strength tends to diminish;

- (2) On average sense, the existing empirical models developed for NAC appear not applicable to the prediction of triaxial behavior of RAC, mainly due to the lack of due considerations on the special and unique characteristics of RCA in those models;
- (3) An empirical design-oriented model for predicting the mechanical properties of RAC under triaxial load is developed based on fitting the test data constructed in this study; statistically, the proposed model outperforms the existing empirical models (i.e., calibrated based on the NAC experimental measurements) in predicting the peak stress and peak strain of RAC under axisymmetric triaxial load;
- (4) The GCA-based evaluations demonstrate that the overall behavior of RAC under triaxial load depends greatly on the exposure temperature, the lateral stress conditions, and the concrete mixture proportions; meanwhile, the effect of RCA replacement ratio is not so remarkable when compared to the other parameters, but this factor is still suggested to be retained in predictive models for a sound and rational interpretation;
- (5) Compared to the other models presented herein, the MNR model and the two neural networks (i.e., the BP-ANN and GA-ANN) developed in a cost-effective manner provide decent fitness in predicting the behavior of RAC under triaxial load, particularly on the peak stress—for the three models, the coefficient of determination range from 0.959 to 0.987, while the mean errors are very limited. Overall, the ANN model optimized with the genetic algorithms performs the best. In view of the above, it is believed that the application of the multivariable regression method and the neural networks may provide well-suited approaches in predicting the triaxial behavior of RAC.

Despite the powerful prediction performance of those artificial intelligence methods exhibited in this study, those methods are acting essentially as a black box and lack of profound physical meaning while generating good outcomes. In this sense, continued efforts are needed to explain the underlying mechanisms why the uniaxial as well as multiaxial behaviors of RAC differ from those of NAC.

Declaration of Competing Interest

None.

Acknowledgements

The research reported in this paper was supported by National Natural Science Foundation of China (Project No: 51708289), Post-doctoral Science Foundation of China (Project No: 2017M611796), Fund of State Key Laboratory of Subtropical Building Science of China (Project Nos: 2018ZB34 and 2019ZB22), Science and Technology Base and Talent Special Project of Guangxi (Project No: AD19110068), Young and Middle-aged Teachers Research Foundation Ability Enhancement Project of Guangxi Universities (Project No: 2019KY0361) and High Level Innovation Group and Outstanding Scholar Program Project of Guangxi High Education (Project No: [2017]38). The authors specially acknowledge the support of Bagui Scholar Program sponsored from the People's Government of Guangxi Zhuang Autonomous Region (Project No: 2019(79)).

Appendix A

Table A1
Experimental database of RAC under axisymmetric triaxial compressions.

Source	Properties of coarse aggregate										Mechanical properties of concrete											
	Concrete mix properties					Properties of coarse aggregate																
	Specimen	D [mm]	H [mm]	T [°C]	σ_3 [MPa]	RCA%	w_{eff}/c	a/c	$\rho_{ad,r}$ [kg/m^3]	$\rho_{hd,n}$ [kg/m^3]	$\rho_{hd,r}$ [kg/m^3]	$\rho_{hd,n}$ [kg/m^3]	W _{RCA} [%]	W _{A_{NA}} [%]	C _{RCA} [%]	C _{A_{NA}} [%]	f_c [MPa]	ϵ_c [10^{-3}]	E _c [GPa]	σ_1 [MPa]	ϵ_1 [10^{-3}]	
Yang et al. [23]	C1	50	100	N/A	0	0	0.40	2.50	N/A	2760	N/A	1429	N/A	1.35	N/A	13	64.36	2.179	N/A	64.36	2.179	
Yang et al. [23]	C1	50	100	N/A	8	0	0.40	2.50	N/A	2760	N/A	1429	N/A	1.35	N/A	13	64.36	2.179	N/A	64.36	2.179	
Yang et al. [23]	C1	50	100	N/A	16	0	0.40	2.50	N/A	2760	N/A	1429	N/A	1.35	N/A	13	64.36	2.179	N/A	64.36	2.179	
Yang et al. [23]	C1	50	100	N/A	24	0	0.40	2.50	N/A	2760	N/A	1429	N/A	1.35	N/A	13	64.36	2.179	N/A	64.36	2.179	
Yang et al. [23]	C1	50	100	N/A	32	0	0.40	2.50	N/A	2760	N/A	1429	N/A	1.35	N/A	13	64.36	2.179	N/A	64.36	2.179	
Yang et al. [23]	C1	50	100	N/A	50	0	0.40	2.50	2430	2760	1260	1429	5.96	1.35	19.5	13	45.21	2.402	N/A	45.21	2.402	
Yang et al. [23]	C1	50	100	N/A	8	50	0.40	2.50	2430	2760	1260	1429	5.96	1.35	19.5	13	45.21	2.402	N/A	45.21	2.402	
Yang et al. [23]	C1	50	100	N/A	16	50	0.40	2.50	2430	2760	1260	1429	5.96	1.35	19.5	13	45.21	2.402	N/A	45.21	2.402	
Yang et al. [23]	C1	50	100	N/A	24	50	0.40	2.50	2430	2760	1260	1429	5.96	1.35	19.5	13	45.21	2.402	N/A	45.21	2.402	
Yang et al. [23]	C1	50	100	N/A	32	50	0.40	2.50	2430	2760	1260	1429	5.96	1.35	19.5	13	45.21	2.402	N/A	45.21	2.402	
Yang et al. [23]	C1	50	100	N/A	0	100	0.40	2.50	2430	N/A	1260	N/A	5.96	N/A	19.5	N/A	47.98	2.520	N/A	47.98	2.520	
Yang et al. [23]	C1	50	100	N/A	8	100	0.40	2.50	2430	N/A	1260	N/A	5.96	N/A	19.5	N/A	47.98	2.520	N/A	47.98	2.520	
Yang et al. [23]	C1	50	100	N/A	16	100	0.40	2.50	2430	N/A	1260	N/A	5.96	N/A	19.5	N/A	47.98	2.520	N/A	47.98	2.520	
Yang et al. [23]	C1	50	100	N/A	24	100	0.40	2.50	2430	N/A	1260	N/A	5.96	N/A	19.5	N/A	47.98	2.520	N/A	47.98	2.520	
Yang et al. [23]	C1	50	100	N/A	32	100	0.40	2.50	2430	N/A	1260	N/A	5.96	N/A	19.5	N/A	47.98	2.520	N/A	47.98	2.520	
Yang et al. [23]	C1	50	100	N/A	0	100	0.40	2.50	2430	N/A	1260	N/A	5.96	N/A	19.5	N/A	47.98	2.520	N/A	47.98	2.520	
Yang et al. [23]	C1	50	100	N/A	8	100	0.40	2.50	2430	N/A	1260	N/A	5.96	N/A	19.5	N/A	47.98	2.520	N/A	47.98	2.520	
Yang et al. [23]	C1	50	100	N/A	16	100	0.40	2.50	2430	N/A	1260	N/A	5.96	N/A	19.5	N/A	47.98	2.520	N/A	47.98	2.520	
Yang et al. [23]	C1	50	100	N/A	24	100	0.40	2.50	2430	N/A	1260	N/A	5.96	N/A	19.5	N/A	47.98	2.520	N/A	47.98	2.520	
Yang et al. [23]	C1	50	100	N/A	32	100	0.40	2.50	2430	N/A	1260	N/A	5.96	N/A	19.5	N/A	47.98	2.520	N/A	47.98	2.520	
Folino and Xargay [24]	C2	100	200	N/A	0	0.50	3.10	N/A	2730	N/A	1109.4	N/A	0.31	N/A	N/A	N/A	36.52	N/A	N/A	36.52	N/A	
Folino and Xargay [24]	C2	100	200	N/A	4.5	0	0.50	3.10	N/A	2730	N/A	1109.4	N/A	0.31	N/A	N/A	N/A	36.52	N/A	N/A	36.52	N/A
Folino and Xargay [24]	C2	100	200	N/A	15	0	0.50	3.10	N/A	2730	N/A	1109.4	N/A	0.31	N/A	N/A	N/A	36.52	N/A	N/A	36.52	N/A
Folino and Xargay [24]	C2	100	200	N/A	21	0	0.50	3.10	N/A	2730	1020	1109.4	2.69	0.31	N/A	N/A	33.59	N/A	N/A	33.59	N/A	
Folino and Xargay [24]	C2	100	200	N/A	0	30	0.52	3.03	2570	2730	1020	1109.4	2.69	0.31	N/A	N/A	33.59	N/A	N/A	33.59	N/A	
Folino and Xargay [24]	C2	100	200	N/A	4.5	30	0.52	3.03	2570	2730	1020	1109.4	2.69	0.31	N/A	N/A	33.59	N/A	N/A	33.59	N/A	
Folino and Xargay [24]	C2	100	200	N/A	4.5	30	0.52	3.03	2570	2730	1020	1109.4	2.69	0.31	N/A	N/A	33.59	N/A	N/A	33.59	N/A	

(continued on next page)

Table A1 (continued)

Source	Geometric properties of specimens			External effect		Concrete mix properties		Properties of coarse aggregate								Mechanical properties of concrete					
	Specimen shape	D [mm]	H [mm]	T [°C]	σ_3 [MPa]	RCA%	w_{eff}/c	a/c	ρ_{adr} [kg/m ³]	$\rho_{ad,n}$ [kg/m ³]	$\rho_{bd,r}$ [kg/m ³]	$\rho_{bd,n}$ [kg/m ³]	WA _{RCA} [%]	WA _{NA} [%]	Cl _{RCA} [%]	Cl _{NA} [%]	f_c [MPa]	ε_o [10 ⁻³]	E _c [GPa]	σ_1 [MPa]	ε_1 [10 ⁻³]
Folino and Xargay [24]	C2	100	200	N/A	15	30	0.52	3.03	2570	2730	1020	1109.4	2.69	0.31	N/A	N/A	33.59	N/A	N/A	88.00	N/A
Folino and Xargay [24]	C2	100	200	N/A	21	30	0.52	3.03	2570	2730	1020	1109.4	2.69	0.31	N/A	N/A	33.59	N/A	N/A	108.29	N/A
Folino and Xargay [24]	C2	100	200	N/A	0	60	0.54	2.95	2570	2730	1020	1109.4	2.69	0.31	N/A	N/A	30.42	N/A	N/A	30.42	N/A
Folino and Xargay [24]	C2	100	200	N/A	4.5	60	0.54	2.95	2570	2730	1020	1109.4	2.69	0.31	N/A	N/A	30.42	N/A	N/A	66.59	N/A
Folino and Xargay [24]	C2	100	200	N/A	15	60	0.54	2.95	2570	2730	1020	1109.4	2.69	0.31	N/A	N/A	30.42	N/A	N/A	84.00	N/A
Folino and Xargay [24]	C2	100	200	N/A	21	60	0.54	2.95	2570	2730	1020	1109.4	2.69	0.31	N/A	N/A	30.42	N/A	N/A	115.00	N/A
Folino and Xargay [24]	C2	100	200	N/A	0	100	0.56	2.85	2570	N/A	1020	N/A	2.69	N/A	N/A	N/A	29.10	N/A	N/A	29.10	N/A
Folino and Xargay [24]	C2	100	200	N/A	4.5	100	0.56	2.85	2570	N/A	1020	N/A	2.69	N/A	N/A	N/A	29.10	N/A	N/A	75.99	N/A
Folino and Xargay [24]	C2	100	200	N/A	15	100	0.56	2.85	2570	N/A	1020	N/A	2.69	N/A	N/A	N/A	29.10	N/A	N/A	87.10	N/A
Folino and Xargay [24]	C2	100	200	N/A	21	100	0.56	2.85	2570	N/A	1020	N/A	2.69	N/A	N/A	N/A	29.10	N/A	N/A	102.74	N/A
Folino and Xargay [24]	C2	100	200	N/A	40	100	0.56	2.85	2570	N/A	1020	N/A	2.69	N/A	N/A	N/A	29.10	N/A	N/A	144.90	N/A
Chen et al. [25]	C2	100	200	N/A	0	0	0.41	2.31	N/A	N/A	N/A	N/A	N/A	N/A	N/A	19.65	4.58	4.60	19.65	4.58	
Chen et al. [25]	C2	100	200	N/A	3	0	0.41	2.31	N/A	N/A	N/A	N/A	N/A	N/A	N/A	19.65	4.58	5.47	41.91	10.76	
Chen et al. [25]	C2	100	200	N/A	6	0	0.41	2.31	N/A	N/A	N/A	N/A	N/A	N/A	N/A	19.65	4.58	7.77	56.08	18.19	
Chen et al. [25]	C2	100	200	N/A	9	0	0.41	2.31	N/A	N/A	N/A	N/A	N/A	N/A	N/A	19.65	4.58	14.93	69.24	16.85	
Chen et al. [25]	C2	100	200	N/A	12	0	0.41	2.31	N/A	N/A	N/A	N/A	N/A	N/A	N/A	19.65	4.58	8.15	82.73	22.17	
Chen et al. [25]	C2	100	200	N/A	15	0	0.41	2.31	N/A	N/A	N/A	N/A	N/A	N/A	N/A	19.65	4.58	6.10	96.76	30.46	
Chen et al. [25]	C2	100	200	N/A	18	0	0.41	2.31	N/A	N/A	N/A	N/A	N/A	N/A	N/A	19.65	4.58	7.83	104.01	40.51	
Chen et al. [25]	C2	100	200	N/A	21	0	0.41	2.31	N/A	N/A	N/A	N/A	N/A	N/A	N/A	19.65	4.58	9.84	114.73	34.75	
Chen et al. [25]	C2	100	200	N/A	24	0	0.41	2.31	N/A	N/A	N/A	N/A	N/A	N/A	N/A	19.65	4.58	13.54	134.88	41.78	
Chen et al. [25]	C2	100	200	N/A	0	30	0.41	2.31	N/A	N/A	N/A	N/A	N/A	N/A	N/A	21.82	3.32	6.92	21.82	3.32	
Chen et al. [25]	C2	100	200	N/A	3	30	0.41	2.31	N/A	N/A	N/A	N/A	N/A	N/A	N/A	21.82	3.32	7.20	43.24	9.11	
Chen et al. [25]	C2	100	200	N/A	6	30	0.41	2.31	N/A	N/A	N/A	N/A	N/A	N/A	N/A	21.82	3.32	7.21	59.03	14.56	
Chen et al. [25]	C2	100	200	N/A	9	30	0.41	2.31	N/A	N/A	N/A	N/A	N/A	N/A	N/A	21.82	3.32	8.37	74.04	18.06	
Chen et al. [25]	C2	100	200	N/A	12	30	0.41	2.31	N/A	N/A	N/A	N/A	N/A	N/A	N/A	21.82	3.32	4.71	89.00	24.12	
Chen et al. [25]	C2	100	200	N/A	15	30	0.41	2.31	N/A	N/A	N/A	N/A	N/A	N/A	N/A	21.82	3.32	15.32	97.00	36.30	
Chen et al. [25]	C2	100	200	N/A	18	30	0.41	2.31	N/A	N/A	N/A	N/A	N/A	N/A	N/A	21.82	3.32	13.21	110.13	34.33	
Chen et al. [25]	C2	100	200	N/A	21	30	0.41	2.31	N/A	N/A	N/A	N/A	N/A	N/A	N/A	21.82	3.32	12.61	126.26	36.53	
Chen et al. [25]	C2	100	200	N/A	24	30	0.41	2.31	N/A	N/A	N/A	N/A	N/A	N/A	N/A	21.82	3.32	17.71	134.23	45.41	
Chen et al. [25]	C2	100	200	N/A	0	70	0.41	2.31	N/A	N/A	N/A	N/A	N/A	N/A	N/A	22.37	3.47	6.06	22.37	3.47	
Chen et al. [25]	C2	100	200	N/A	3	70	0.41	2.31	N/A	N/A	N/A	N/A	N/A	N/A	N/A	22.37	3.47	7.16	45.17	8.55	
Chen et al. [25]	C2	100	200	N/A	6	70	0.41	2.31	N/A	N/A	N/A	N/A	N/A	N/A	N/A	22.37	3.47	14.75	61.04	9.13	
Chen et al. [25]	C2	100	200	N/A	9	70	0.41	2.31	N/A	N/A	N/A	N/A	N/A	N/A	N/A	22.37	3.47	5.73	75.05	19.47	
Chen et al. [25]	C2	100	200	N/A	12	70	0.41	2.31	N/A	N/A	N/A	N/A	N/A	N/A	N/A	22.37	3.47	12.57	80.60	23.28	
Chen et al. [25]	C2	100	200	N/A	15	70	0.41	2.31	N/A	N/A	N/A	N/A	N/A	N/A	N/A	22.37	3.47	8.93	99.21	35.09	
Chen et al. [25]	C2	100	200	N/A	18	70	0.41	2.31	N/A	N/A	N/A	N/A	N/A	N/A	N/A	22.37	3.47	11.67	100.97	38.36	
Chen et al. [25]	C2	100	200	N/A	21	70	0.41	2.31	N/A	N/A	N/A	N/A	N/A	N/A	N/A	22.37	3.47	11.80	112.03	37.49	
Chen et al. [25]	C2	100	200	N/A	24	70	0.41	2.31	N/A	N/A	N/A	N/A	N/A	N/A	N/A	22.37	3.47	15.76	127.32	42.86	
Chen et al. [25]	C2	100	200	N/A	0	100	0.41	2.31	N/A	N/A	N/A	N/A	N/A	N/A	N/A	19.04	3.81	4.71	19.04	3.81	
Chen et al. [25]	C2	100	200	N/A	3	100	0.41	2.31	N/A	N/A	N/A	N/A	N/A	N/A	N/A	19.04	3.81	9.25	38.98	7.81	
Chen et al. [25]	C2	100	200	N/A	6	100	0.41	2.31	N/A	N/A	N/A	N/A	N/A	N/A	N/A	19.04	3.81	9.65	57.14	8.18	
Chen et al. [25]	C2	100	200	N/A	9	100	0.41	2.31	N/A	N/A	N/A	N/A	N/A	N/A	N/A	19.04	3.81	9.65	75.29	19.9	
Chen et al. [25]	C2	100	200	N/A	12	100	0.41	2.31	N/A	N/A	N/A	N/A	N/A	N/A	N/A	19.04	3.81	8.31	85.84	20.38	
Chen et al. [25]	C2	100	200	N/A	15	100	0.41	2.31	N/A	N/A	N/A	N/A	N/A	N/A	N/A	19.04	3.81	13.51	94.61	31.54	
Chen et al. [25]	C2	100	200	N/A	18	100	0.41	2.31	N/A	N/A	N/A	N/A	N/A	N/A	N/A	19.04	3.81	11.97	107.38	41.85	
Chen et al. [25]	C2	100	200	N/A	21	100	0.41	2.31	N/A	N/A	N/A	N/A	N/A	N/A	N/A	19.04	3.81	14.30	118.67	38.64	
Chen et al. [25]	C2	100	200	N/A	24	100	0.41	2.31	N/A	N/A	N/A	N/A	N/A	N/A	N/A	19.04	3.81	16.47	134.22	43.64	
Chen et al. [25]	C2	100	200	N/A	27	100	0.41	2.31	N/A	N/A	N/A	N/A	N/A	N/A	N/A	19.04	3.81	6.79	147.03	49.64	
Chen et al. [25]	C2	100	200	N/A	0	0	0.32	1.50	N/A	N/A	N/A	N/A	N/A	N/A	N/A	31.11	4.04	8.33	31.11	4.04	
Chen et al. [25]	C2	100	200	N/A	6	0	0.32	1.50	N/A	N/A	N/A	N/A	N/A	N/A	N/A	31.11	4.04	11.58	69.28	7.62	
Chen et al. [25]	C2	100	200	N/A	12	0	0.32	1.50	N/A	N/A	N/A	N/A	N/A	N/A	N/A	31.11	4.04	11.05	100.49	16.45	
Chen et al. [25]	C2	100	200	N/A	0	30	0.32	1.50	N/A	N/A	N/A	N/A	N/A	N/A	N/A	31.68	4.08	7.85	31.68	4.08	

Chen et al. [25]	C2	100	200	N/A	6	30	0.32	1.50	N/A	N/A	N/A	N/A	N/A	N/A	N/A	31.68	4.08	8.26	78.69	11.61	
Chen et al. [25]	C2	100	200	N/A	12	30	0.32	1.50	N/A	N/A	N/A	N/A	N/A	N/A	N/A	31.68	4.08	16.34	108.38	11.04	
Chen et al. [25]	C2	100	200	N/A	0	70	0.32	1.50	N/A	N/A	N/A	N/A	N/A	N/A	N/A	31.35	4.25	8.81	31.35	4.25	
Chen et al. [25]	C2	100	200	N/A	6	70	0.32	1.50	N/A	N/A	N/A	N/A	N/A	N/A	N/A	31.35	4.25	7.01	71.49	12.30	
Chen et al. [25]	C2	100	200	N/A	12	70	0.32	1.50	N/A	N/A	N/A	N/A	N/A	N/A	N/A	31.35	4.25	13.71	98.04	14.59	
Chen et al. [25]	C2	100	200	N/A	0	100	0.32	1.50	N/A	N/A	N/A	N/A	N/A	N/A	N/A	31.68	4.08	8.81	31.68	4.08	
Chen et al. [25]	C2	100	200	N/A	6	100	0.32	1.50	N/A	N/A	N/A	N/A	N/A	N/A	N/A	31.68	4.08	8.75	66.15	13.42	
Chen et al. [25]	C2	100	200	N/A	12	100	0.32	1.50	N/A	N/A	N/A	N/A	N/A	N/A	N/A	31.68	4.08	10.93	100.69	14.91	
Chen et al. [25]	C2	100	200	N/A	0	100	0.41	2.31	N/A	N/A	N/A	N/A	N/A	N/A	N/A	23.33	2.96	8.12	23.33	2.96	
Chen et al. [25]	C2	100	200	N/A	3	100	0.41	2.31	N/A	N/A	N/A	N/A	N/A	N/A	N/A	23.33	2.96	7.66	52.45	8.25	
Chen et al. [25]	C2	100	200	N/A	6	100	0.41	2.31	N/A	N/A	N/A	N/A	N/A	N/A	N/A	23.33	2.96	6.49	62.77	11.53	
Chen et al. [25]	C2	100	200	N/A	9	100	0.41	2.31	N/A	N/A	N/A	N/A	N/A	N/A	N/A	23.33	2.96	5.34	78.58	17.26	
Chen et al. [25]	C2	100	200	N/A	12	100	0.41	2.31	N/A	N/A	N/A	N/A	N/A	N/A	N/A	23.33	2.96	6.91	93.77	24.32	
Chen et al. [25]	C2	100	200	N/A	15	100	0.41	2.31	N/A	N/A	N/A	N/A	N/A	N/A	N/A	23.33	2.96	7.59	106.39	21.61	
Chen et al. [25]	C2	100	200	N/A	0	100	0.41	2.31	N/A	N/A	N/A	N/A	N/A	N/A	N/A	23.82	3.62	6.29	23.82	3.62	
Chen et al. [25]	C2	100	200	N/A	3	100	0.41	2.31	N/A	N/A	N/A	N/A	N/A	N/A	N/A	23.82	3.62	9.02	53.23	7.37	
Chen et al. [25]	C2	100	200	N/A	6	100	0.41	2.31	N/A	N/A	N/A	N/A	N/A	N/A	N/A	23.82	3.62	7.62	62.45	14.56	
Chen et al. [25]	C2	100	200	N/A	9	100	0.41	2.31	N/A	N/A	N/A	N/A	N/A	N/A	N/A	23.82	3.62	11.59	76.88	19.98	
Chen et al. [25]	C2	100	200	N/A	12	100	0.41	2.31	N/A	N/A	N/A	N/A	N/A	N/A	N/A	23.82	3.62	15.57	87.67	17.02	
Chen et al. [25]	C2	100	200	N/A	15	100	0.41	2.31	N/A	N/A	N/A	N/A	N/A	N/A	N/A	23.82	3.62	10.44	100.04	25.47	
Meng et al. [26]	C2	100	200	N/A	0	0	0.41	2.15	N/A	2652	N/A	1523	N/A	0.88	N/A	N/A	14.42	N/A	N/A	14.42	N/A
Meng et al. [26]	C2	100	200	N/A	5	0	0.41	2.15	N/A	2652	N/A	1523	N/A	0.88	N/A	N/A	14.42	N/A	N/A	56.09	N/A
Meng et al. [26]	C2	100	200	N/A	10	0	0.41	2.15	N/A	2652	N/A	1523	N/A	0.88	N/A	N/A	14.42	N/A	N/A	77.96	N/A
Meng et al. [26]	C2	100	200	N/A	15	0	0.41	2.15	N/A	2652	N/A	1523	N/A	0.88	N/A	N/A	14.42	N/A	N/A	95.70	N/A
Meng et al. [26]	C2	100	200	N/A	20	0	0.41	2.15	N/A	2652	N/A	1523	N/A	0.88	N/A	N/A	14.42	N/A	N/A	121.39	N/A
Meng et al. [26]	C2	100	200	N/A	0	30	0.41	2.15	2359	2652	1347	1523	6.5	0.88	N/A	N/A	16.15	N/A	N/A	16.15	N/A
Meng et al. [26]	C2	100	200	N/A	5	30	0.41	2.15	2359	2652	1347	1523	6.5	0.88	N/A	N/A	16.15	N/A	N/A	56.85	N/A
Meng et al. [26]	C2	100	200	N/A	10	30	0.41	2.15	2359	2652	1347	1523	6.5	0.88	N/A	N/A	16.15	N/A	N/A	78.30	N/A
Meng et al. [26]	C2	100	200	N/A	15	30	0.41	2.15	2359	2652	1347	1523	6.5	0.88	N/A	N/A	16.15	N/A	N/A	96.74	N/A
Meng et al. [26]	C2	100	200	N/A	20	30	0.41	2.15	2359	2652	1347	1523	6.5	0.88	N/A	N/A	16.15	N/A	N/A	117.5	N/A
Meng et al. [26]	C2	100	200	N/A	0	70	0.41	2.15	2359	2652	1347	1523	6.5	0.88	N/A	N/A	11.38	N/A	N/A	11.38	N/A
Meng et al. [26]	C2	100	200	N/A	5	70	0.41	2.15	2359	2652	1347	1523	6.5	0.88	N/A	N/A	11.38	N/A	N/A	53.22	N/A
Meng et al. [26]	C2	100	200	N/A	10	70	0.41	2.15	2359	2652	1347	1523	6.5	0.88	N/A	N/A	11.38	N/A	N/A	73.86	N/A
Meng et al. [26]	C2	100	200	N/A	15	70	0.41	2.15	2359	2652	1347	1523	6.5	0.88	N/A	N/A	11.38	N/A	N/A	97.43	N/A
Meng et al. [26]	C2	100	200	N/A	20	70	0.41	2.15	2359	2652	1347	1523	6.5	0.88	N/A	N/A	11.38	N/A	N/A	114.95	N/A
Meng et al. [26]	C2	100	200	N/A	0	100	0.41	2.15	2359	N/A	1347	N/A	6.5	N/A	N/A	12.62	N/A	N/A	12.62	N/A	
Meng et al. [26]	C2	100	200	N/A	5	100	0.41	2.15	2359	N/A	1347	N/A	6.5	N/A	N/A	12.62	N/A	N/A	50.34	N/A	
Meng et al. [26]	C2	100	200	N/A	10	100	0.41	2.15	2359	N/A	1347	N/A	6.5	N/A	N/A	12.62	N/A	N/A	71.64	N/A	
Meng et al. [26]	C2	100	200	N/A	15	100	0.41	2.15	2359	N/A	1347	N/A	6.5	N/A	N/A	12.62	N/A	N/A	97.04	N/A	
Meng et al. [26]	C2	100	200	N/A	20	100	0.41	2.15	2359	N/A	1347	N/A	6.5	N/A	N/A	12.62	N/A	N/A	114.08	N/A	
Meng et al. [26]	C2	100	200	200	0	0	0.41	2.15	N/A	2652	N/A	1523	N/A	0.88	N/A	N/A	9.88	N/A	N/A	9.88	N/A
Meng et al. [26]	C2	100	200	200	5	0	0.41	2.15	N/A	2652	N/A	1523	N/A	0.88	N/A	N/A	9.88	N/A	N/A	48.74	N/A
Meng et al. [26]	C2	100	200	200	10	0	0.41	2.15	N/A	2652	N/A	1523	N/A	0.88	N/A	N/A	9.88	N/A	N/A	80.82	N/A
Meng et al. [26]	C2	100	200	200	15	0	0.41	2.15	N/A	2652	N/A	1523	N/A	0.88	N/A	N/A	9.88	N/A	N/A	94.44	N/A
Meng et al. [26]	C2	100	200	200	20	0	0.41	2.15	N/A	2652	N/A	1523	N/A	0.88	N/A	N/A	9.88	N/A	N/A	114.12	N/A
Meng et al. [26]	C2	100	200	200	0	30	0.41	2.15	2359	2652	1347	1523	6.5	0.88	N/A	N/A	10.25	N/A	N/A	10.25	N/A
Meng et al. [26]	C2	100	200	200	5	30	0.41	2.15	2359	2652	1347	1523	6.5	0.88	N/A	N/A	10.25	N/A	N/A	48.11	N/A
Meng et al. [26]	C2	100	200	200	10	30	0.41	2.15	2359	2652	1347	1523	6.5	0.88	N/A	N/A	10.25	N/A	N/A	69.68	N/A
Meng et al. [26]	C2	100	200	200	15	30	0.41	2.15	2359	2652	1347	1523	6.5	0.88	N/A	N/A	10.25	N/A	N/A	86.55	N/A
Meng et al. [26]	C2	100	200	200	20	30	0.41	2.15	2359	2652	1347	1523	6.5	0.88	N/A	N/A	10.25	N/A	N/A	107.35	N/A
Meng et al. [26]	C2	100	200	200	0	70	0.41	2.15	2359	2652	1347	1523	6.5	0.88	N/A	N/A	12.45	N/A	N/A	12.45	N/A
Meng et al. [26]	C2	100	200	200	5	70	0.41	2.15	2359	2652	1347	1523	6.5	0.88	N/A	N/A	12.45	N/A	N/A	54.16	N/A
Meng et al. [26]	C2	100	200	200	10	70	0.41	2.15	2359	2652	1347	1523	6.5	0.88	N/A	N/A	12.45	N/A	N/A	71.76	N/A
Meng et al. [26]	C2	100	200	200	15	70	0.41	2.15	2359	2652	1347	1523	6.5	0.88	N/A	N/A	12.45	N/A	N/A	98.34	N/A
Meng et al. [26]	C2	100	200	200	20	70	0.41	2.15	2359	2652	1347	1523	6.5	0.88	N/A	N/A	12.45	N/A	N/A	114.12	N/A
Meng et al. [26]	C2	100	200	200	0	100	0.41	2.15	2359	N/A	1347	N/A	6.5	N/A	N/A	15.89	N/A	N/A	15.89	N/A	
Meng et al. [26]	C2	100	200	200	5	100	0.41	2.15	2359	N/A	1347	N/A	6.5	N/A	N/A	15.89	N/A	N/A	48.15	N/A	
Meng et al. [26]	C2	100	200	200	10	100	0.41	2.15	2359	N/A	1347	N/A	6.5	N/A	N/A	15.89	N/A	N/A	76.19	N/A	
Meng et al. [26]	C2	100	200	200	15	100	0.41	2.15	2359	N/A	1347	N/A	6.5	N/A	N/A	15.89	N/A	N/A	84.73	N/A	
Meng et al. [26]	C2	100	200	200	20	100	0.41	2.15	2359	N/A	1347	N/A	6.5	N/A	N/A	15.89	N/A	N/A	106.49	N/A	

(continued on next page)

Table A1 (continued)

Source	Geometric properties of specimens			External effect		Concrete mix properties			Properties of coarse aggregate								Mechanical properties of concrete				
	Specimen shape	D [mm]	H [mm]	T [°C]	σ_3 [MPa]	RCA%	w_{eff}/c	a/c	$\rho_{ad,r}$ [kg/m³]	$\rho_{ad,n}$ [kg/m³]	$\rho_{bd,r}$ [kg/m³]	$\rho_{bd,n}$ [kg/m³]	WA _{RCA} [%]	WA _{NA} [%]	C _{RCA} [%]	C _{NA} [%]	f_c [MPa]	ε_o [10⁻³]	E _c [GPa]	σ_1 [MPa]	ε_1 [10⁻³]
Meng et al. [26]	C2	100	200	300	0	0	0.41	2.15	N/A	2652	N/A	1523	N/A	0.88	N/A	N/A	9.45	N/A	N/A	9.45	N/A
Meng et al. [26]	C2	100	200	300	5	0	0.41	2.15	N/A	2652	N/A	1523	N/A	0.88	N/A	N/A	9.45	N/A	N/A	48.81	N/A
Meng et al. [26]	C2	100	200	300	10	0	0.41	2.15	N/A	2652	N/A	1523	N/A	0.88	N/A	N/A	9.45	N/A	N/A	77.37	N/A
Meng et al. [26]	C2	100	200	300	15	0	0.41	2.15	N/A	2652	N/A	1523	N/A	0.88	N/A	N/A	9.45	N/A	N/A	97.39	N/A
Meng et al. [26]	C2	100	200	300	20	0	0.41	2.15	N/A	2652	N/A	1523	N/A	0.88	N/A	N/A	9.45	N/A	N/A	117.07	N/A
Meng et al. [26]	C2	100	200	300	0	30	0.41	2.15	2359	2652	1347	1523	6.5	0.88	N/A	N/A	10.65	N/A	N/A	10.65	N/A
Meng et al. [26]	C2	100	200	300	5	30	0.41	2.15	2359	2652	1347	1523	6.5	0.88	N/A	N/A	10.65	N/A	N/A	46.43	N/A
Meng et al. [26]	C2	100	200	300	10	30	0.41	2.15	2359	2652	1347	1523	6.5	0.88	N/A	N/A	10.65	N/A	N/A	74.32	N/A
Meng et al. [26]	C2	100	200	300	15	30	0.41	2.15	2359	2652	1347	1523	6.5	0.88	N/A	N/A	10.65	N/A	N/A	92.35	N/A
Meng et al. [26]	C2	100	200	300	20	30	0.41	2.15	2359	2652	1347	1523	6.5	0.88	N/A	N/A	10.65	N/A	N/A	114.54	N/A
Meng et al. [26]	C2	100	200	300	0	70	0.41	2.15	2359	2652	1347	1523	6.5	0.88	N/A	N/A	11.59	N/A	N/A	11.59	N/A
Meng et al. [26]	C2	100	200	300	5	70	0.41	2.15	2359	2652	1347	1523	6.5	0.88	N/A	N/A	11.59	N/A	N/A	46.28	N/A
Meng et al. [26]	C2	100	200	300	10	70	0.41	2.15	2359	2652	1347	1523	6.5	0.88	N/A	N/A	11.59	N/A	N/A	77.77	N/A
Meng et al. [26]	C2	100	200	300	15	70	0.41	2.15	2359	2652	1347	1523	6.5	0.88	N/A	N/A	11.59	N/A	N/A	99.49	N/A
Meng et al. [26]	C2	100	200	300	20	70	0.41	2.15	2359	2652	1347	1523	6.5	0.88	N/A	N/A	11.59	N/A	N/A	114.54	N/A
Meng et al. [26]	C2	100	200	300	0	100	0.41	2.15	2359	N/A	1347	N/A	6.5	N/A	N/A	9.34	N/A	N/A	9.34	N/A	
Meng et al. [26]	C2	100	200	300	5	100	0.41	2.15	2359	N/A	1347	N/A	6.5	N/A	N/A	9.34	N/A	N/A	45.16	N/A	
Meng et al. [26]	C2	100	200	300	10	100	0.41	2.15	2359	N/A	1347	N/A	6.5	N/A	N/A	9.34	N/A	N/A	65.03	N/A	
Meng et al. [26]	C2	100	200	300	15	100	0.41	2.15	2359	N/A	1347	N/A	6.5	N/A	N/A	9.34	N/A	N/A	95.79	N/A	
Meng et al. [26]	C2	100	200	300	20	100	0.41	2.15	2359	N/A	1347	N/A	6.5	N/A	N/A	9.34	N/A	N/A	107.40	N/A	
Meng et al. [26]	C2	100	200	400	0	0	0.41	2.15	N/A	2652	N/A	1523	N/A	0.88	N/A	N/A	9.33	N/A	N/A	9.33	N/A
Meng et al. [26]	C2	100	200	400	5	0	0.41	2.15	N/A	2652	N/A	1523	N/A	0.88	N/A	N/A	9.33	N/A	N/A	52.89	N/A
Meng et al. [26]	C2	100	200	400	10	0	0.41	2.15	N/A	2652	N/A	1523	N/A	0.88	N/A	N/A	9.33	N/A	N/A	80.06	N/A
Meng et al. [26]	C2	100	200	400	15	0	0.41	2.15	N/A	2652	N/A	1523	N/A	0.88	N/A	N/A	9.33	N/A	N/A	102.40	N/A
Meng et al. [26]	C2	100	200	400	20	0	0.41	2.15	N/A	2652	N/A	1523	N/A	0.88	N/A	N/A	9.33	N/A	N/A	120.99	N/A
Meng et al. [26]	C2	100	200	400	0	30	0.41	2.15	2359	2652	1347	1523	6.5	0.88	N/A	N/A	13.86	N/A	N/A	13.86	N/A
Meng et al. [26]	C2	100	200	400	5	30	0.41	2.15	2359	2652	1347	1523	6.5	0.88	N/A	N/A	13.86	N/A	N/A	53.22	N/A
Meng et al. [26]	C2	100	200	400	10	30	0.41	2.15	2359	2652	1347	1523	6.5	0.88	N/A	N/A	13.86	N/A	N/A	71.75	N/A
Meng et al. [26]	C2	100	200	400	15	30	0.41	2.15	2359	2652	1347	1523	6.5	0.88	N/A	N/A	13.86	N/A	N/A	90.58	N/A
Meng et al. [26]	C2	100	200	400	20	30	0.41	2.15	2359	2652	1347	1523	6.5	0.88	N/A	N/A	13.86	N/A	N/A	103.59	N/A
Meng et al. [26]	C2	100	200	400	0	70	0.41	2.15	2359	2652	1347	1523	6.5	0.88	N/A	N/A	8.34	N/A	N/A	8.34	N/A
Meng et al. [26]	C2	100	200	400	5	70	0.41	2.15	2359	2652	1347	1523	6.5	0.88	N/A	N/A	8.34	N/A	N/A	51.15	N/A
Meng et al. [26]	C2	100	200	400	10	70	0.41	2.15	2359	2652	1347	1523	6.5	0.88	N/A	N/A	8.34	N/A	N/A	71.66	N/A
Meng et al. [26]	C2	100	200	400	15	70	0.41	2.15	2359	2652	1347	1523	6.5	0.88	N/A	N/A	8.34	N/A	N/A	94.38	N/A
Meng et al. [26]	C2	100	200	400	20	70	0.41	2.15	2359	2652	1347	1523	6.5	0.88	N/A	N/A	8.34	N/A	N/A	114.54	N/A
Meng et al. [26]	C2	100	200	400	0	100	0.41	2.15	2359	N/A	1347	N/A	6.5	N/A	N/A	16.90	N/A	N/A	16.90	N/A	
Meng et al. [26]	C2	100	200	400	5	100	0.41	2.15	2359	N/A	1347	N/A	6.5	N/A	N/A	16.90	N/A	N/A	46.46	N/A	
Meng et al. [26]	C2	100	200	400	10	100	0.41	2.15	2359	N/A	1347	N/A	6.5	N/A	N/A	16.90	N/A	N/A	71.21	N/A	
Meng et al. [26]	C2	100	200	400	15	100	0.41	2.15	2359	N/A	1347	N/A	6.5	N/A	N/A	16.90	N/A	N/A	93.52	N/A	
Meng et al. [26]	C2	100	200	400	20	100	0.41	2.15	2359	N/A	1347	N/A	6.5	N/A	N/A	16.90	N/A	N/A	106.53	N/A	
Meng et al. [26]	C2	100	200	500	0	0	0.41	2.15	N/A	2652	N/A	1523	N/A	0.88	N/A	N/A	11.16	N/A	N/A	11.16	N/A
Meng et al. [26]	C2	100	200	500	5	0	0.41	2.15	N/A	2652	N/A	1523	N/A	0.88	N/A	N/A	11.16	N/A	N/A	48.65	N/A
Meng et al. [26]	C2	100	200	500	10	0	0.41	2.15	N/A	2652	N/A	1523	N/A	0.88	N/A	N/A	11.16	N/A	N/A	78.49	N/A
Meng et al. [26]	C2	100	200	500	15	0	0.41	2.15	N/A	2652	N/A	1523	N/A	0.88	N/A	N/A	11.16	N/A	N/A	98.23	N/A
Meng et al. [26]	C2	100	200	500	20	0	0.41	2.15	N/A	2652	N/A	1523	N/A	0.88	N/A	N/A	11.16	N/A	N/A	116.08	N/A
Meng et al. [26]	C2	100	200	500	0	30	0.41	2.15	2359	2652	1347	1523	6.5	0.88	N/A	N/A	7.84	N/A	N/A	7.84	N/A
Meng et al. [26]	C2	100	200	500	5	30	0.41	2.15	2359	2652	1347	1523	6.5	0.88	N/A	N/A	7.84	N/A	N/A	47.68	N/A
Meng et al. [26]	C2	100	200	500	10	30	0.41	2.15	2359	2652	1347	1523	6.5	0.88	N/A	N/A	7.84	N/A	N/A	71.02	N/A
Meng et al. [26]	C2	100	200	500	15	30	0.41	2.15	2359	2652	1347	1523	6.5	0.88	N/A	N/A	7.84	N/A	N/A	93.92	N/A
Meng et al. [26]	C2	100	200	500	20	30	0.41	2.15	2359	2652	1347	1523	6.5	0.88	N/A	N/A	7.84	N/A	N/A	107.83	N/A
Meng et al. [26]	C2	100	200	500	0	70	0.41	2.15	2359	2652	1347	1523	6.5	0.88	N/A	N/A	7.31	N/A	N/A	7.31	N/A
Meng et al. [26]	C2	100	200	500	5	70	0.41	2.15	2359	2652	1347	1523	6.5	0.88	N/A	N/A	7.31	N/A	N/A	53.56	N/A
Meng et al. [26]	C2	100	200	500	10	70	0.41	2.15	2359	2652	1347	1523	6.5	0.88	N/A	N/A	7.31	N/A	N/A	76.07	N/A
Meng et al. [26]	C2	100	200	500	15	70	0.41	2.15	2359	2652	1347	1523	6.5	0.88	N/A	N/A	7.31	N/A	N/A	93.92	N/A

Table A2

Experimental database of RAC under true triaxial compressions.

Source	Geometric properties of specimens			Stress conditions		Concrete mix properties		Properties of coarse aggregate						Mechanical properties of concrete							
	Specimen type	B [mm]	H [mm]	$\sigma_3:\sigma_1$	$\sigma_2:\sigma_1$	RCA%	W_{eff}/c	a/c	$\rho_{ad,r}$ [kg/m ³]	$\rho_{ad,n}$ [kg/m ³]	$\rho_{bd,r}$ [kg/m ³]	$\rho_{bd,n}$ [kg/m ³]	WA _{RCA} [%]	WA _{NA} [%]	Cl _{RCA} [%]	Cl _{NA} [%]	f'_c [MPa]	ε_o [10 ⁻³]	E_c [GPa]	σ_1 [MPa]	ε_1 [10 ⁻³]
He et al. [27]	S2	150	150	0	0	30	0.40	3.17	2560	2720	1350	1470	2.91	0.56	11.42	3.89	22.85	N/A	N/A	22.85	N/A
He et al. [27]	S2	150	150	0	1	30	0.40	3.17	2560	2720	1350	1470	2.91	0.56	11.42	3.89	22.85	N/A	N/A	32.19	N/A
He et al. [27]	S2	150	150	0.1	0.1	30	0.40	3.17	2560	2720	1350	1470	2.91	0.56	11.42	3.89	22.85	N/A	N/A	71.19	N/A
He et al. [27]	S2	150	150	0.1	0.25	30	0.40	3.17	2560	2720	1350	1470	2.91	0.56	11.42	3.89	22.85	N/A	N/A	96.40	N/A
He et al. [27]	S2	150	150	0.1	0.5	30	0.40	3.17	2560	2720	1350	1470	2.91	0.56	11.42	3.89	22.85	N/A	N/A	112.02	N/A
He et al. [27]	S2	150	150	0.1	0.75	30	0.40	3.17	2560	2720	1350	1470	2.91	0.56	11.42	3.89	22.85	N/A	N/A	109.26	N/A
He et al. [27]	S2	150	150	0.1	1	30	0.40	3.17	2560	2720	1350	1470	2.91	0.56	11.42	3.89	22.85	N/A	N/A	97.32	N/A
He et al. [27]	S2	150	150	0	0	50	0.37	3.13	2560	2720	1350	1470	2.91	0.56	11.42	3.89	27.74	N/A	N/A	27.74	N/A
He et al. [27]	S2	150	150	0	1	50	0.37	3.13	2560	2720	1350	1470	2.91	0.56	11.42	3.89	27.74	N/A	N/A	39.93	N/A
He et al. [27]	S2	150	150	0.1	0.1	50	0.37	3.13	2560	2720	1350	1470	2.91	0.56	11.42	3.89	27.74	N/A	N/A	90.39	N/A
He et al. [27]	S2	150	150	0.1	0.25	50	0.37	3.13	2560	2720	1350	1470	2.91	0.56	11.42	3.89	27.74	N/A	N/A	103.36	N/A
He et al. [27]	S2	150	150	0.1	0.5	50	0.37	3.13	2560	2720	1350	1470	2.91	0.56	11.42	3.89	27.74	N/A	N/A	107.40	N/A
He et al. [27]	S2	150	150	0.1	0.75	50	0.37	3.13	2560	2720	1350	1470	2.91	0.56	11.42	3.89	27.74	N/A	N/A	112.77	N/A
He et al. [27]	S2	150	150	0.1	1	50	0.37	3.13	2560	2720	1350	1470	2.91	0.56	11.42	3.89	27.74	N/A	N/A	102.65	N/A
He et al. [28]	S2	150	150	0	0	30	0.30	2.35	2560	2720	1350	1470	2.91	0.56	11.42	3.89	30.68	N/A	N/A	30.68	N/A
He et al. [28]	S2	150	150	0	1	30	0.30	2.35	2560	2720	1350	1470	2.91	0.56	11.42	3.89	30.68	N/A	N/A	38.39	N/A
He et al. [28]	S2	150	150	0.1	0.1	30	0.30	2.35	2560	2720	1350	1470	2.91	0.56	11.42	3.89	30.68	N/A	N/A	89.61	N/A
He et al. [28]	S2	150	150	0.1	0.25	30	0.30	2.35	2560	2720	1350	1470	2.91	0.56	11.42	3.89	30.68	N/A	N/A	104.22	N/A
He et al. [28]	S2	150	150	0.1	0.5	30	0.30	2.35	2560	2720	1350	1470	2.91	0.56	11.42	3.89	30.68	N/A	N/A	110.81	N/A
He et al. [28]	S2	150	150	0.1	0.75	30	0.30	2.35	2560	2720	1350	1470	2.91	0.56	11.42	3.89	30.68	N/A	N/A	107.92	N/A
He et al. [28]	S2	150	150	0.1	1	30	0.30	2.35	2560	2720	1350	1470	2.91	0.56	11.42	3.89	30.68	N/A	N/A	108.64	N/A
He et al. [28]	S2	150	150	0	0	30	0.40	3.17	2560	2720	1350	1470	2.91	0.56	11.42	3.89	22.85	N/A	N/A	22.85	N/A
He et al. [28]	S2	150	150	0	1	30	0.40	3.17	2560	2720	1350	1470	2.91	0.56	11.42	3.89	22.85	N/A	N/A	32.19	N/A
He et al. [28]	S2	150	150	0.1	0.1	30	0.40	3.17	2560	2720	1350	1470	2.91	0.56	11.42	3.89	22.85	N/A	N/A	71.19	N/A
He et al. [28]	S2	150	150	0.1	0.25	30	0.40	3.17	2560	2720	1350	1470	2.91	0.56	11.42	3.89	22.85	N/A	N/A	96.40	N/A
He et al. [28]	S2	150	150	0.1	0.5	30	0.40	3.17	2560	2720	1350	1470	2.91	0.56	11.42	3.89	22.85	N/A	N/A	112.02	N/A
He et al. [28]	S2	150	150	0.1	0.75	30	0.40	3.17	2560	2720	1350	1470	2.91	0.56	11.42	3.89	22.85	N/A	N/A	109.26	N/A
He et al. [28]	S2	150	150	0.1	1	30	0.40	3.17	2560	2720	1350	1470	2.91	0.56	11.42	3.89	22.85	N/A	N/A	97.32	N/A
He et al. [28]	S2	150	150	0	0	30	0.51	4.75	2560	2720	1350	1470	2.91	0.56	11.42	3.89	15.50	N/A	N/A	15.50	N/A
He et al. [28]	S2	150	150	0	1	30	0.51	4.75	2560	2720	1350	1470	2.91	0.56	11.42	3.89	15.50	N/A	N/A	20.27	N/A
He et al. [28]	S2	150	150	0.1	0.1	30	0.51	4.75	2560	2720	1350	1470	2.91	0.56	11.42	3.89	15.50	N/A	N/A	39.20	N/A
He et al. [28]	S2	150	150	0.1	0.25	30	0.51	4.75	2560	2720	1350	1470	2.91	0.56	11.42	3.89	15.50	N/A	N/A	53.73	N/A
He et al. [28]	S2	150	150	0.1	0.5	30	0.51	4.75	2560	2720	1350	1470	2.91	0.56	11.42	3.89	15.50	N/A	N/A	61.88	N/A
He et al. [28]	S2	150	150	0.1	0.75	30	0.51	4.75	2560	2720	1350	1470	2.91	0.56	11.42	3.89	15.50	N/A	N/A	60.62	N/A
He et al. [28]	S2	150	150	0.1	1	30	0.51	4.75	2560	2720	1350	1470	2.91	0.56	11.42	3.89	15.50	N/A	N/A	53.90	N/A
Deng et al. [29]	S1	100	100	0.1	0.25	0	0.47	2.70	N/A	2708	N/A	N/A	N/A	0.30	N/A	4.6	N/A	N/A	N/A	244.15	N/A
Deng et al. [29]	S1	100	100	0.1	0.5	0	0.47	2.70	N/A	2708	N/A	N/A	N/A	0.30	N/A	4.6	N/A	N/A	N/A	273.80	N/A
Deng et al. [29]	S1	100	100	0.1	0.75	0	0.47	2.70	N/A	2708	N/A	N/A	N/A	0.30	N/A	4.6	N/A	N/A	N/A	253.53	N/A
Deng et al. [29]	S1	100	100	0.1	1	0	0.47	2.70	N/A	2708	N/A	N/A	N/A	0.30	N/A	4.6	N/A	N/A	N/A	222.38	N/A
Deng et al. [29]	S1	100	100	0.1	0.25	30	0.46	2.64	2485	2708	N/A	N/A	3.00	0.30	13.4	4.6	N/A	N/A	N/A	249.06	N/A
Deng et al. [29]	S1	100	100	0.1	0.5	30	0.46	2.64	2485	2708	N/A	N/A	3.00	0.30	13.4	4.6	N/A	N/A	N/A	280.23	N/A
Deng et al. [29]	S1	100	100	0.1	0.75	30	0.46	2.64	2485	2708	N/A	N/A	3.00	0.30	13.4	4.6	N/A	N/A	N/A	264.45	N/A
Deng et al. [29]	S1	100	100	0.1	1	30	0.46	2.64	2485	2708	N/A	N/A	3.00	0.30	13.4	4.6	N/A	N/A	N/A	226.70	N/A
Deng et al. [29]	S1	100	100	0.1	0.25	50	0.45	2.58	2485	2708	N/A	N/A	3.00	0.30	13.4	4.6	N/A	N/A	N/A	217.70	N/A
Deng et al. [29]	S1	100	100	0.1	0.5	50	0.45	2.58	2485	2708	N/A	N/A	3.00	0.30	13.4	4.6	N/A	N/A	N/A	235.57	N/A
Deng et al. [29]	S1	100	100	0.1	0.75	50	0.45	2.58	2485	2708	N/A	N/A	3.00	0.30	13.4	4.6	N/A	N/A	N/A	228.77	N/A
Deng et al. [29]	S1	100	100	0.1	1	50	0.45	2.58	2485	2708	N/A	N/A	3.00	0.30	13.4	4.6	N/A	N/A	N/A	198.73	N/A
Deng et al. [29]	S1	100	100	0.1	0.25	70	0.44	2.52	2485	2708	N/A	N/A	3.00	0.30	13.4	4.6	N/A	N/A	N/A	205.66	N/A
Deng et al. [29]	S1	100	100	0.1	0.5	70	0.44	2.52	2485	2708	N/A	N/A	3.00	0.30	13.4	4.6	N/A	N/A	N/A	212.49	N/A
Deng et al. [29]	S1	100	100	0.1	0.75	70	0.44	2.52	2485	2708	N/A	N/A	3.00	0.30	13.4	4.6	N/A	N/A	N/A	209.42	N/A
Deng et al. [29]	S1	100	100	0.1	1	70	0.44	2.52	2485	2708	N/A	N/A	3.00	0.30	13.4	4.6	N/A	N/A	N/A	181.64	N/A

(continued on next page)

References

- [1] J.J. Xu, Z.P. Chen, X.Y. Zhao, C. Demartino, T. Ozbakkaloglu, J.Y. Xue, Seismic performance of circular recycled aggregate concrete-filled steel tubular columns: FEM modelling and sensitivity analysis, *Thin-Walled Struct.* 141 (2019) 509–525.
- [2] Z.P. Chen, J.J. Xu, Y.L. Chen, E.M. Lui, Recycling and reuse of construction and demolition waste in concrete-filled steel tubes: a review, *Constr. Build. Mater.* 126 (2016) 641–660.
- [3] J.J. Xu, Z.P. Chen, Y. Xiao, C. Demartino, J.H. Wang, Recycled aggregate concrete in FRP-confined columns: a review of experimental results, *Compos. Struct.* 174 (2017) 277–291.
- [4] T.Y. Xie, A. Gholampour, T. Ozbakkaloglu, Toward the development of sustainable concretes with recycled concrete aggregates: comprehensive review of studies on mechanical properties, *J. Mater. Civ. Eng.* 30 (9) (2018) 04018211.
- [5] R.V. Silva, A. Silva, R. Neves, J.de. Brito, Statistical modeling of carbonation in concrete incorporating recycled aggregates, *J. Mater. Civ. Eng.* 28 (1) (2016) 04015082.
- [6] T. Uygunoğlu, İ.B. Topçu, A.G. Çelik, Use of waste marble and recycled aggregates in self-compacting concrete for environmental sustainability, *J. Cleaner Prod.* 84 (2014) 691–700.
- [7] G. Fathifazl, A. Abbas, A.G. Razaqpur, O.B. Isgor, B. Fournier, S. Foo, New mixture proportioning method for concrete made with coarse recycled concrete aggregate, *J. Mater. Civ. Eng.* 21 (10) (2009) 601–611.
- [8] L.P. Rosado, P. Vitalé, C.S.G. Penteado, U. Arena, Life cycle assessment of natural and mixed recycled aggregate production in Brazil, *J. Cleaner Prod.* 151 (2017) 634–642.
- [9] V. Corinaldesi, G. Moriconi, Behaviour of cementitious mortars containing different kinds of recycled aggregate, *Constr. Build. Mater.* 23 (1) (2009) 289–294.
- [10] L. Ferreira, J.de. Brito, M. Barra, Influence of the pre-saturation of recycled coarse concrete aggregates on concrete properties, *Mag. Concr. Res.* 63 (8) (2011) 617–627.
- [11] R.V. Silva, J.de. Brito, R.K. Dhir, The influence of the use of recycled aggregates on the compressive strength of concrete: a review, *Eur. J. Environ. Civ. Eng.* 19 (7) (2015) 825–849.
- [12] H.Z. Cui, X. Shi, S.A. Memon, F. Xing, W. Tang, Experimental study on the influence of water absorption of recycled coarse aggregates on properties of the resulting concretes, *J. Mater. Civ. Eng.* 27 (4) (2015) 04014138.
- [13] A. Abbas, G. Fathifazl, B. Fournier, O.B. Isgord, R. Zavadile, A.G. Razaqpur, S. Foo, Quantification of the residual mortar content in recycled concrete aggregates by image analysis, *Mater. Charact.* 60 (7) (2009) 716–72811.
- [14] D. Pedro, J.de. Brito, L. Evangelista, Performance of concrete made with aggregates recycled from precasting industry waste: influence of the crushing process, *Mater. Struct.* 48 (12) (2015) 3965–3978.
- [15] A.F.M.S. Amin, A. Hasnat, A.H. Khan, M. Ashiquzzaman, Residual cementing property in recycled fines and coarse aggregates: occurrence and quantification, *J. Mater. Civ. Eng.* 28 (4) (2016) 04015174.
- [16] F. Ceia, J. Raposo, M. Guerra, E. Júlio, J.de. Brito, Shear strength of recycled aggregate concrete to natural aggregate concrete interfaces, *Constr. Build. Mater.* 109 (2016) 139–145.
- [17] Y.F. Yang, L.H. Han, Experimental behaviour of recycled aggregate concrete filled steel tubular columns, *J. Constr. Steel Res.* 62 (12) (2006) 1310–1324.
- [18] Y.X. Liu, X.X. Zha, G.B. Gong, Study on recycled-concrete-filled steel tube and recycled concrete based on damage mechanics, *J. Constr. Steel Res.* 71 (2012) 143–148.
- [19] Y.Y. Wang, J. Chen, Y. Geng, Testing and analysis of axially loaded normal-strength recycled aggregate filled steel tubular stub columns, *Eng. Struct.* 86 (2015) 192–212.
- [20] J.Z. Xiao, Y.J. Huang, J. Yang, C. Zhang, Mechanical properties of confined recycled aggregate concrete under axial compression, *Constr. Build. Mater.* 26 (1) (2012) 591–603.
- [21] J.L. Zhao, T. Yu, J.G. Teng, Stress-strain behavior of FRP-confined recycled aggregate concrete, *ASCE J. Compos. Constr.* 19 (3) (2014) 04014054.
- [22] T.Y. Xie, T. Ozbakkaloglu, Behavior of recycled aggregate concrete-filled basalt and carbon FRP tubes, *Constr. Build. Mater.* 105 (2016) 132–143.
- [23] H.F. Yang, S.P. Meng, Z.H. Deng, Stress-strain curves of high-performance recycled concrete under conventional triaxial compression, *J. Jiangsu Univ. (Nat. Sci. Ed.)* 32 (5) (2011) 597–601.
- [24] P. Folino, H. Xargay, Recycled aggregate concrete—mechanical behavior under uniaxial and triaxial compression, *Constr. Build. Mater.* 56 (3) (2014) 21–31.
- [25] Z.P. Chen, Y.L. Chen, J.J. Xu, J.Y. Xue, Experimental study on failure criterion and stress-strain constitutive equation of recycled coarse aggregate concretes under multiaxial compression, *China Civ. Eng. J.* 48 (12) (2015) 23–33.
- [26] E.C. Meng, Y.L. Yu, J. Yuan, K. Qiao, Y.S. Su, Triaxial compressive strength experiment study of recycled aggregate concrete after high temperatures, *Constr. Build. Mater.* 155 (2017) 542–549.
- [27] Z.J. He, J.X. Zhang, Strength characteristics and failure criterion of plain recycled aggregate concrete under triaxial stress states, *Constr. Build. Mater.* 54 (11) (2014) 354–362.
- [28] Z.J. He, W.L. Cao, J.X. Zhang, L. Wang, Multiaxial mechanical properties of plain recycled aggregate concrete, *Mag. Concr. Res.* 67 (8) (2015) 1–13.

Table A2 (continued)

Source	Geometric properties of specimens		Stress conditions		Concrete mix properties		Properties of coarse aggregate						Mechanical properties of concrete							
	Specimen type	B [mm]	H [mm]	σ_3 : σ_1	σ_2 : σ_1	RCA%	w_{eff}/c	q/c	$\rho_{ad,r}$ [kg/m ³]	$\rho_{ad,t}$ [kg/m ³]	$\rho_{bd,r}$ [kg/m ³]	$\rho_{bd,t}$ [kg/m ³]	W_{RCA} [%]	W_{NA} [%]	C_{RCA} [%]	C_{NA} [%]	f_c [MPa]	ε_o [10^{-3}]	E_c [GPa]	σ_1 [MPa]
Deng et al. [29]	S1	100	100	0.1	0.25	100	0.43	2.46	2485	N/A	N/A	N/A	3.00	N/A	13.4	N/A	N/A	187.44	N/A	N/A
Deng et al. [29]	S1	100	100	0.1	0.5	100	0.43	2.46	2485	N/A	N/A	N/A	3.00	N/A	13.4	N/A	N/A	200.83	N/A	N/A
Deng et al. [29]	S1	100	100	0.1	0.75	100	0.43	2.46	2485	N/A	N/A	N/A	3.00	N/A	13.4	N/A	N/A	192.10	N/A	N/A
Deng et al. [29]	S1	100	100	0.1	1	100	0.43	2.46	2485	N/A	N/A	N/A	3.00	N/A	13.4	N/A	N/A	170.00	N/A	N/A

- [29] Z.H. Deng, Y.M. Wang, J. Sheng, X. Hu, Strength and deformation of recycled aggregate concrete under triaxial compression, *Constr. Build. Mater.* 156 (2017) 1043–1052.
- [30] E. Richart, A. Brandtzaeg, R.L. Brown, Failure of plain and spirally reinforced concrete in compression. Bulletin 190, University of Illinois Engineering Experimental Station, Champaign, IL, 1929.
- [31] G.G. Balmer, Shearing strength of concrete under high triaxial stress—Computation of Mohr's envelope as a curve, Report SP-23, Structural Research Laboratory, U.S. Bureau of Reclamation, Denver, 1949.
- [32] J. Chinn, R.M. Zimmerman, Behavior of plain concrete under various high triaxial compression loading conditions, Technical Rep. No. WL TR 64-163, University of Colorado, Denver, 1965.
- [33] C. Avram, R.E. Fadacaru, I. Filimon, O. Mirsu, I. Terteia, *Concrete Strength and Strains*, Elsevier Scientific, Amsterdam, 1981, pp. 156–178.
- [34] S. Martinez, A.H. Nilson, F.O. Slate, Spirally reinforced high-strength concrete columns, *J. Am. Concr. Inst.* 81 (5) (1984) 431–442.
- [35] M. Saatcioglu, S.R. Razvi, Strength and ductility of confined concrete, *J. Struct. Eng.* 118 (6) (1992) 1590–1607.
- [36] S. Setunge, M.M. Attard, P. Darvall, Ultimate strength of confined very high-strength concretes, *ACI Struct. J.* 90 (6) (1993) 632–641.
- [37] J. Xie, A.E. Elwi, J.G. MacGregor, Mechanical properties of three high-strength concretes containing silica fume, *ACI Mater. J.* 92 (2) (1995) 135–145.
- [38] M.M. Attard, S. Setunge, Stress-strain relationship of confined and unconfined concrete, *ACI Mater. J.* 93 (5) (1996) 432–442.
- [39] S. Lan, Z. Guo, Experimental investigation of multiaxial compressive strength of concrete under different stress paths, *ACI Mater. J.* 94 (5) (1997) 427–434.
- [40] F. Ansari, Q. Li, High-strength concrete subjected to triaxial compression, *ACI Mater. J.* 95 (6) (1998) 747–755.
- [41] M. Samaan, A. Mirmiran, M. Shahawy, Model of concrete confined by fiber composites, *J. Struct. Eng.* 124 (9) (1998) 1025–1031.
- [42] Q. Li, F. Ansari, High-strength concrete in triaxial compression by different sizes of specimens, *ACI Mater. J.* 97 (6) (2000) 684–689.
- [43] D.C. Candappa, J.G. Sanjayan, S. Setunge, Complete triaxial stress-strain curves of high-strength concrete, *J. Mater. Civ. Eng.* 13 (3) (2001) 209–215.
- [44] M. Saatcioglu, S.R. Razvi, Displacement-based design of reinforced concrete columns for confinement, *ACI Struct. J.* 99 (1) (2002) 3–11.
- [45] F. Légeron, P. Paultre, Uniaxial confinement model for normal-and high-strength concrete columns, *J. Struct. Eng.* 129 (2) (2003) 241–252.
- [46] Z.C. Girgin, N. Arioglu, E. Arioglu, Evaluation of strength criteria for very-high-strength concretes under triaxial compression, *ACI Struct. J.* 104 (3) (2007) 278–284.
- [47] O. Bohwan, L. Myung-Ho, P. Sang-John, Experimental study of 60 MPa concrete under triaxial stress, in: Structural Engineers World Congress (SEWC), Bangalore, India, 2007.
- [48] C.W. Tang, Radial basis function neural network models for peak stress and strain in plain concrete under triaxial stress, *J. Mater. Civ. Eng.* 22 (9) (2010) 923–934.
- [49] A.K. Samani, M.M. Attard, A stress-strain model for uniaxial and confined concrete under compression, *Eng. Struct.* 41 (3) (2012) 335–349.
- [50] İ.B. Topçu, M. Saridemir, Prediction of mechanical properties of recycled aggregate concretes containing silica fume using artificial neural networks and fuzzy logic, *Comput. Mater. Sci.* 42 (1) (2008) 74–82.
- [51] C.Y. Chang, R. Huang, P.C. Lee, T.L. Weng, Application of a weighted grey-taguchi method for optimizing recycled aggregate concrete mixtures, *Cem. Concr. Compos.* 33 (10) (2011) 1038–1049.
- [52] Z.H. Duan, S.C. Kou, C.S. Poon, Prediction of compressive strength of recycled aggregate concrete using artificial neural networks, *Constr. Build. Mater.* 40 (7) (2013) 1200–1206.
- [53] Z.H. Duan, S.C. Kou, C.S. Poon, Using artificial neural networks for predicting the elastic modulus of recycled aggregate concrete, *Constr. Build. Mater.* 44 (7) (2013) 524–532.
- [54] A.T.A. Dantas, M.B. Leite, K.D.J. Nagahama, Prediction of compressive strength of concrete containing construction and demolition waste using artificial neural networks, *Constr. Build. Mater.* 38 (2) (2013) 717–722.
- [55] I. González-Taboada, B. González-Fonteboa, F. Martínez-Abella, J.L. Pérez-Ordóñez, Prediction of the mechanical properties of structural recycled concrete using multivariable regression and genetic proGCAmming, *Constr. Build. Mater.* 106 (2016) 480–499.
- [56] F. Deng, Y. He, S. Zhou, Y. Yu, H. Cheng, X. Wu, Compressive strength prediction of recycled concrete based on deep learning, *Constr. Build. Mater.* 175 (2018) 562–569.
- [57] A. Behnood, J. Olek, M.A. Glinicki, Predicting modulus elasticity of recycled aggregate concrete using m5' model tree algorithm, *Constr. Build. Mater.* 94 (2015) 137–147.
- [58] M. Velay-Lizancos, J.L. Perez-OrdoEZ, I. Martinez-Lage, P. Vazquez-Burgo, Analytical and genetic proGCAmming model of compressive strength of eco concretes by NDT according to curing temperature, *Constr. Build. Mater.* 144 (2017) 195–206.
- [59] E.M. Golafshani, A. Behnood, Application of soft computing methods for predicting the elastic modulus of recycled aggregate concrete, *J. Cleaner Prod.* 176 (2018) 1163–1176.
- [60] J.J. Xu, X.Y. Zhao, Y. Yu, T.Y. Xie, G.S. Yang, J.Y. Xue, Parametric sensitivity analysis and modelling of mechanical properties of normal- and high-strength recycled aggregate concrete using grey theory, multiple nonlinear regression and artificial neural networks, *Constr. Build. Mater.* 211 (2019) 479–491.
- [61] S.F. Liu, Y.J. Yang, J. Forrest, *Grey Data Analysis: Methods, Models and Applications*, Springer, Singapore, 2017.
- [62] J.J. Xu, Z.P. Chen, T. Ozbakkaloglu, X.Y. Zhao, C. Demartino, A critical assessment of the compressive behavior of reinforced recycled aggregate concrete columns, *Eng. Struct.* 161 (2018) 161–175.
- [63] F. Wang, Y. Yu, X.Y. Zhao, J.J. Xu, T.Y. Xie, S.T. Deresa, Performance evaluation of reinforced recycled aggregate concrete columns under cyclic loadings, *Appl. Sci.* 9 (7) (2019) 1460–1461.
- [64] FIB, fib Model Code for Concrete Structures 2010, International Federation for Structural Concrete (fib), Lausanne, 2013.
- [65] C.J. Zega, A.A.D. Maio, Recycled concrete exposed to high temperatures, *Mag. Concr. Res.* 58 (10) (2006) 675–682.
- [66] Y. Li, H. Yi, J. Wu, L. Xu, Sensitivity analysis of recycled concrete based on grey model, *Rev. Téc. Ing. Univ. Zulia.* 39 (11) (2016) 118–124.
- [67] I. Imran, S.J. Pantazopoulou, Plasticity model for concrete under triaxial compression, *J. Eng. Mech.* 127 (3) (2001) 281–290.
- [68] J. Pu, S. Ding, B. He, Study of the behavior of concrete under triaxial compression, *J. Eng. Mech.* 128 (2) (2002) 156–163.
- [69] M.G. Alexander, T.I. Milne, Influence of cement blend and aggregate type on stress-strain behavior and elastic modulus of concrete, *ACI Mater. J.* 92 (3) (1995) 227–235.
- [70] J.M. Chi, R. Huang, C.C. Yang, J.J. Chang, Effect of aggregate properties on the strength and stiffness of lightweight concrete, *Cem. Concr. Compos.* 25 (2) (2003) 197–205.
- [71] R.S. Ravindrarajah, C.T. Tam, Properties of concrete made with crushed concrete as coarse aggregate, *Mag. Concr. Res.* 37 (130) (1985) 29–38.
- [72] N.K. Bairagi, K. Ravande, V.K. Pareek, Behaviour of concrete with different proportions of natural and recycled aggregates, *Resour. Conserv. Recycl.* 9 (1) (1993) 109–126.
- [73] R.K. Dhir, Sustainability of recycled concrete aggregate for use in BS 5328 designated mixes, *Proc. Inst. Civ. Eng.-Struct. Build.* 134 (3) (1999) 257–274.
- [74] G.F. Kheder, S.A. Al-Windawi, Variation in mechanical properties of natural and recycled aggregate concrete as related to the strength of their binding mortar, *Mater. Struct.* 38 (7) (2005) 701–709.
- [75] J.Z. Xiao, P. Li, W. Qin, Study on bond-slip between recycled concrete and rebars, *J. Tongji Univ.* 34 (1) (2006) 13–16.
- [76] P.S. Lovato, E. Possan, D.C.C. Dal Molin, A.B. Masuero, J.L.D. Ribeiro, Modeling of mechanical properties and durability of recycled aggregate concretes, *Constr. Build. Mater.* 26 (1) (2012) 437–447.
- [77] P. Pereira, L. Evangelista, J.de. Brito, The effect of superplasticisers on the workability and compressive strength of concrete made with fine recycled concrete aggregates, *Constr. Build. Mater.* 28 (2012) 722–729.
- [78] P. Pereira, L. Evangelista, J.de. Brito, The effect of superplasticizers on the mechanical performance of concrete made with fine recycled concrete aggregates, *Cement Concr. Compos.* 34 (9) (2012) 1044–1052.
- [79] A. Gholampour, A.H. Gandomi, T. Ozbakkaloglu, New formulations for mechanical properties of recycled aggregate concrete using gene expression proGCAmming, *Constr. Build. Mater.* 130 (2017) 122–145.
- [80] H. Scheffé, Experiments with mixtures, *J. Roy. Stat. Soc.* 20 (2) (1958) 344–360.
- [81] M.T. Hagan, M. Beale, M. Beale, *Neural Network Design*, Machine Press, China, 2002.
- [82] G. Dreyfus, *Neural Networks: Methodology and Applications*, Springer-Verlag, Berlin Heidelberg, 2005.
- [83] N. Siddique, H. Adeli, *Computational Intelligence: Synergies of Fuzzy Logic, Neural Networks and Evolutionary Computing*, John Wiley & Sons, 2013.
- [84] J.L. McClelland, D.E. Rumelhart, *Parallel Distributed Processing, Volume 2: Psychological and Biological Models*, The MIT Press, Cambridge, MA, 1986.
- [85] S.L. Hung, H. Adeli, Object-oriented backpropagation and its application to structural design, *Neurocomputing* 6 (1) (1994) 45–55.
- [86] H. Adeli, Neural networks in civil engineering: 1989–2000, *Comput.-Aided Civ. Infrastruct. Eng.* 16 (2) (2001) 126–142.
- [87] S. Lai, M. Serra, Concrete strength prediction by means of neural network, *Constr. Build. Mater.* 11 (2) (1997) 93–98.
- [88] I.C. Yeh, Modeling of strength of high-performance concrete using artificial neural networks, *Cem. Concr. Res.* 28 (12) (1998) 1797–1808.
- [89] İ.B. Topçu, M. Saridemir, Prediction of properties of waste AAC aggregate concrete using artificial neural network, *Comput. Mater. Sci.* 41 (1) (2008) 117–125.
- [90] E. Ghafari, M. Bandarabadi, H. Costa, E. Júlio, Prediction of fresh and hardened state properties of UHPC: comparative study of statistical mixture design and an artificial neural network model, *J. Mater. Civ. Eng.* 27 (11) (2015) 04015017.
- [91] L.D. Chambers, *Practical Handbook of Genetic Algorithms: Complex Coding Systems*, CRC Press, 1998.
- [92] V. Chandwani, V. Agrawal, R. Nagar, Modeling slump of ready mix concrete using genetic algorithms assisted training of Artificial Neural Networks, *Expert Syst. Appl.* 42 (2) (2015) 885–893.
- [93] S. Akkurt, S. Ozdemir, G. Tayfur, B. Akyol, The use of GA-ANNs in the modelling of compressive strength of cement mortar, *Cem. Concr. Res.* 33 (7) (2003) 973–979.
- [94] S. Sadati, L.E.B. da Silva, I.I. Wunsch, C. Donald, K.H. Khayat, Artificial intelligence to investigate modulus of elasticity of recycled aggregate concrete, *ACI Mater. J.* 116 (1) (2019) 51–62.
- [95] D.E. Goldberg, *Genetic Algorithm in Search, Optimization and Machine Learning*, Addison-Wesley, 1989.

- [96] D.J. Higham, N.J. Higham, MATLAB Guide, SIAM, Philadelphia, 2016.
- [97] E.M. Güneyisi, M. Geçoğlu, E. Güneyisi, K. Mermerdaş, Assessment of shear capacity of adhesive anchors for structures using neural network based model, *Mater. Struct.* 49 (3) (2016) 1065–1077.
- [98] M.Y. Cheng, D. Prayogo, Y.W. Wu, Novel genetic algorithm-based evolutionary support vector machine for optimizing high-performance concrete mixture, *J. Comput. Civil Eng.* 28 (4) (2013) 06014003.
- [99] C.G. Looney, Advances in feedforward neural networks: demystifying knowledge acquiring black boxes, *IEEE Trans. Knowl. Data Eng.* 2 (1996) 211–226.
- [100] K.T. Yücel, C. Özal, Modeling of mechanical properties and bond relationship using data mining process, *Adv. Eng. Softw.* 45 (1) (2012) 54–60.